A REMEDIAL APPROACH TO STABILIZE A DEEP EXCAVATION IN SINGAPORE

By

Alessia Alexandra Ferrari

Laurea, Ingegneria Civile-Strutture
Università di Brescia- Italy

Submitted to the Department of
Civil and Environmental Engineering in
Partial Fulfillment of the Requirements for the Degree of

Master of Engineering in
Civil and Environmental Engineering
at the

Massachusetts Institute of Technology

February 2007

Signature of Author:_____
Department of Civil and Environmental Engineering
January 19,2007

Certified by:_____
Andrew J. Whittle
Professor of Civil and Environmental Engineering
Thesis Supervisor

Accepted by:_____
Andrew J. Whittle
Professor of Civil and Environmental Engineering
Chairman, Departmental Committee for Graduate Students

A REMEDIAL APPROACH TO STABILIZE

A DEEP EXCAVATION IN SINGAPORE

By

Alessia A. Ferrari

Submitted to the department of Civil and Environmental Engineering on January 19, 2007 in Partial Fulfillment of the Requirements for the Degree of Master of Engineering in Civil and Environmental Engineering

Abstract

Ground improvement methods are commonly adopted in deep excavation to minimize wall deflection, wall bending moment and strut force. In this thesis a different approach to the application of ground improvement techniques is analyzed in the form of a parametric study developed with the use of a commercial finite element code. A new remedial ground improvement solution applied to an existing deep excavation located in Singapore and part of the Circle Line Project (CCL) for the construction of a new subway line is considered and computationally modeled. The soil profile in the site mainly consists of deep marine soft clay dated for the most part in the Holocene period, principally characterized by a normally to very low overconsolidation ratio, in some location even underconsolidated. The parametric analysis aims to evaluate short-term effects of the application of cementing agents to the lower portion of the marine clay externally to the excavation side. The effectiveness of the proposed ground improvement is examined using a finite element model corresponding to a key cross-section of CCL1 project. Parametric analyses are used to assess how the dimensions of the treatment zone and strength of soilcrete columns affect the computed wall deflections, bending moments and strut loads. The results demonstrate the validity of the proposed method in controlling the structural behavior of the excavation support system. The same method is then used to simulate the retrofit of the partially excavated section. The results show it is possible for an external ground treatment to control wall deflections and bending moments and reduce strut loads. The thesis finally discuss the practical advantages of the solution and its limitations.

Thesis Supervisor: Andrew J. Whittle

Title: Professor of Civil and Environmental Engineering

Acknowledgments

I would like to thank my Professor Andrew J. Whittle for his support, guidance and wealth of knowledge which he gave me during this experience at MIT.

I would like also to extend my deepest gratitude to my family which has always supported me in every big or small step of my life. In particular I am profoundly thankful to my father Tullio, for being a constant model for me and who made this fantastic experience possible. I could never thank them enough for the constant love they always give me.

It is also necessary to thank all the MEng students 2005-2006 because they add something special to this already wonderful experience. In particular I cannot forget Rossella, the best roommate ever, always ready to help me whatever I needed and sincere confident during the difficult moments, Aurelie, just because she is great, Irene, Claire, Dimitris, Simos and Juan.

Of course I cannot forget all the friends of the third floor, the Geotechnical group, and in particular Naeem Abdulhadi who made my last year at MIT special and unique.

Thanks to you all, this intense, even though short, experience will stay in my memory forever.

Table of Contents

List of Tables

List of Figures

1. INTRODUCTION

In the past decades the city of Singapore has been involved in a major development process which has included the construction of an extensive subway network (Figure 1.1).

The $6.7 billion Circle Line Project (CCL) comprises 33.6 km long underground subway which was scheduled to completion in 2009 with 26 operating stations.

Due to the complexity of the project and to time issues, the entire line has be divided in 5 different stages of construction.

The first stage here proposed (CCL1) goes from Dhoby Ghaut to Boulevard station covering a total length of 5.4 km with 6 stations and originally scheduled to be completed in 2006.

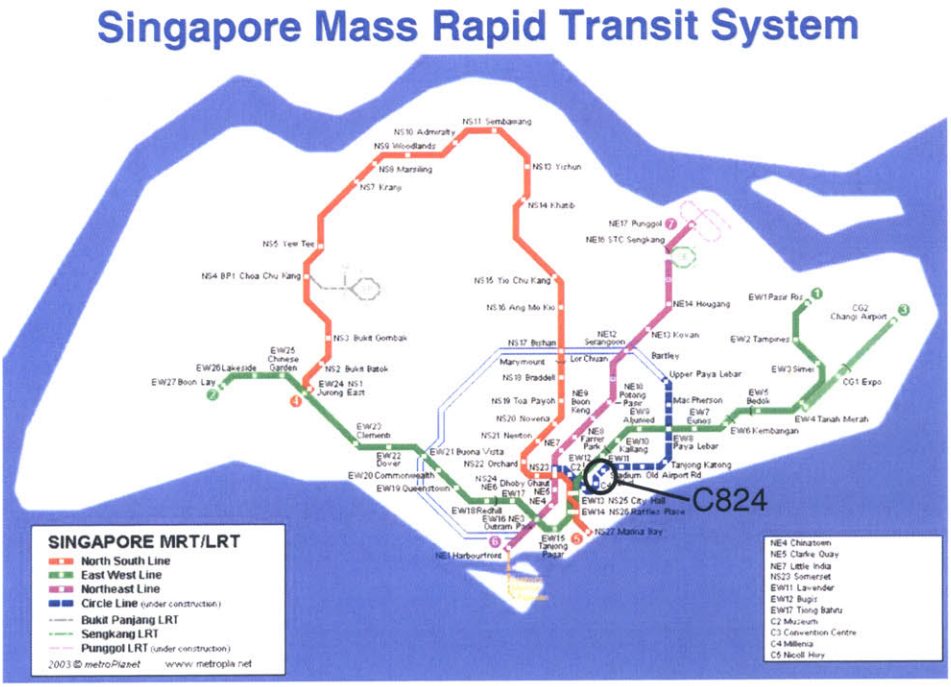

Figure 1.1- Map of Singapore Mass Rapid Transit System

This stage has been in its turn divided in two contracts namely C824 and C825; C824 contract has an overall route length of 2.8 km, and consists in a cut and cover portion of the alignment connecting twin bored tunnels passing underneath Kallang Basin and two underground stations: Nicoll Highway and Boulevard Station.

In such a densely populated urban area it is extremely important to control the magnitude of lateral wall deflections and the corresponding ground movement during construction (Peck 1969; Clough and O'Rourke 1990) to avoid potential damage to nearby structures. Different measures can be adopted to control excavation-induced movements including strengthening the bracing system and increasing the passive resistance of the excavation support system e.g. using cross-lot barettes, deep mixing or jet grouting.

This thesis considers the use of deep soil improvement techniques for controlling movements around deep excavation in Singapore Marine Clay (MC).
This remediation technique is specifically examined for ground conditions encountered in contract C824 of the first phase of the Circle Line Project in Singapore. This is the location where a major collapse occurred in 2004 (Nicoll Highway Collapse, COI, 2005). The subway excavations in this area are more than 30 m deep and occur within 40 m of soft marine clay deposits.

Jet grout rafts are widely used (ref. Appendix A) to reinforce deep excavations by increasing the passive resistance of the soil beneath the foundation level and predominant feature at the site of the Nicoll Highway Collapse.

This thesis applies a different concept. Here the structural performance of the excavation support system is improved reducing the active pressure acting on the diaphragm wall; this is here obtained increasing the undrained shear strength of the soil treating it in the external part of the excavation.

The contribution of the ground improvement to the overall stability of the structure is evaluated in the form of a sensitivity analysis through a series of numerical analysis (the finite element method) to assess its effect on reducing diaphragm wall displacements, bending moments, struts loads and ground surface settlements.
The analyses are performed using computer software, Plaxis 2-D (*PLAXIS* v.8.2, http://www.plaxis.nl accessed on 2/1/2007).

This thesis is divided into four main sections:

1. Detailed description of the local ground conditions and excavation support system for contact C824 of the Circle Line project in Singapore.
2. Presentation of numerical simulations used to investigate key parameters controlling the effectiveness of the proposed ground treatment.
3. A careful discussion on the practical meaning of the results obtained with emphasis in the role of the finite element model affecting the results, its limitations in relation to the structural behavior of the typical elements of the excavation such as diaphragm wall, struts and jet grout slab located at bottom level.
4. Application for remediation of C824 section type K.

2. DEEP EXCAVATION SUPPORT SYSTEM FOR CONTRACT C824

2.1 General Layout

Figure 2.1 shows the layout of the Circle Line contract with eight different zones: Cut and Cover 1 (CC1), Nicoll Highway Station (NCH), Crossover Box tunnel (XOB), Cut and Cover 2 (CC2), Temporary Staging Area (TSA), Launch Shaft 1 (LS1), Boulevard Station (BLV) and Boulevard Siding (BLS).

Circle Line Phase 1: Contract C824

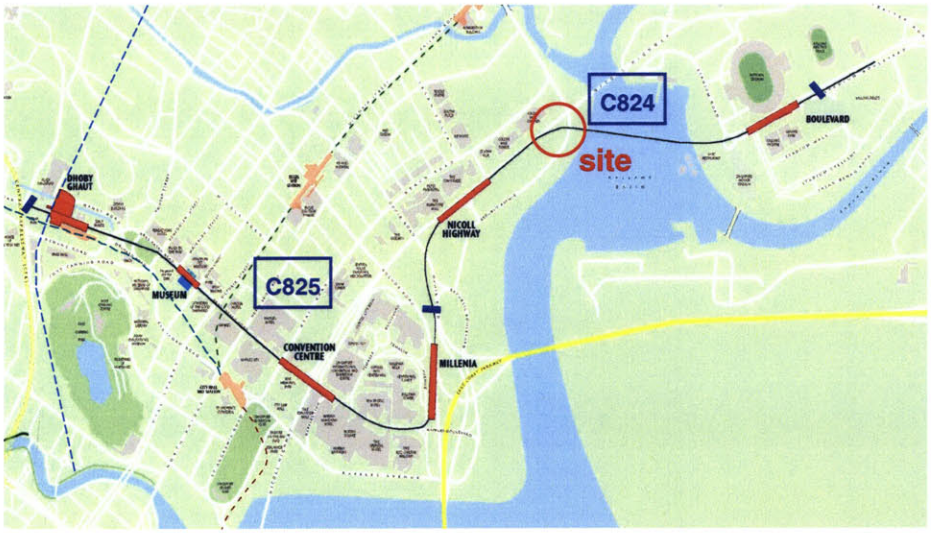

Figure 2.1- Map of Circle Line Project and detail of CCL1 in Singapore

This contract includes 2 km of cut-and-cover excavation and about 800 m of twin bored tunnels running beneath the Kallang River.

Figure 2.2 shows the typical excavation support system, permanent works and ground conditions in section CCL1 at the location of the collapse (Type M3), close to the TSA access shaft. At this location the excavation is approximately 20 m wide and up to 33 m deep. The permanent works include two rectangular tunnel boxes supported in drilled shafts (bored piles). The excavation

support system comprises 0.8 m thick diaphragm wall panels (typically 6-7 m long) which are embedded up to 3 m in the underlying Old Alluvium (at depths exceeding 40 m). At this section the original design included 10 levels of cross-lot bracing and two layers/rafts of jet grout pile support (JGP) 1.6 m and 2.6 m thick, respectively. These JGP layers are installed prior to excavation and are primarily intended to strength the passive resistance of the lower marine clay and estuarine units. The upper JGP is a sacrificial layer that was to be removed as the M3 excavation proceeded below the 9th level of strutting.

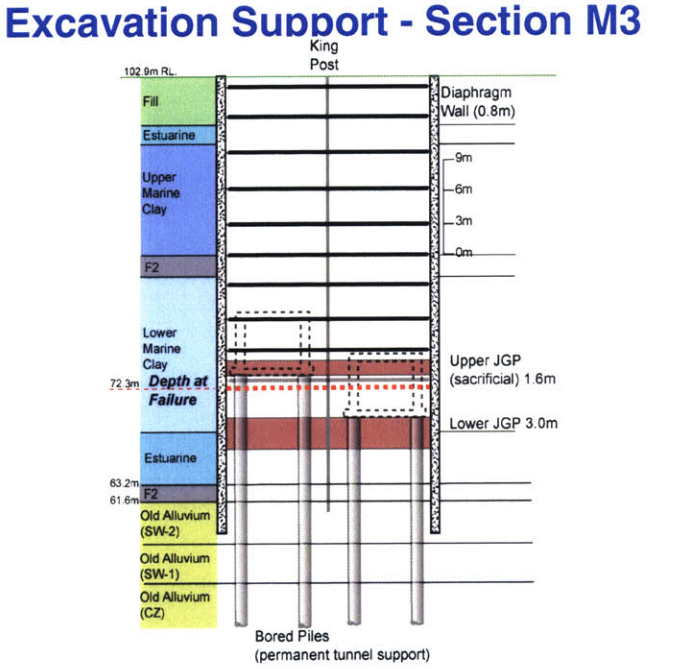

Figure 2.2- Typical excavation support system for section type M3, part of CCL1

(Whittle and Davis,2006)

Collapse of the Nicoll Highway occurred due to a catastrophic failure of the bracing system at M3. This thesis is principally concerned with evaluating an alternative technique for improving the performance of the excavation support system using externally applied JGP rafts. For this purpose, the principal focus is on the performance of the support system of section K, close to the junction between the cross over box (XOB) and CC2. Chapter 4 describe the use of the proposed external JGP as a component of the excavation support system at section K, while Chapter 5 illustrates how external JGP could be used to retrofit/remediate the partially excavated

section K following the collapse of the Nicoll Highway. The following section describes the remediation of the partially completed excavations for C824.

There are a series of high-rise buildings are high-rise buildings (the Plaza, Plaza Park Royal, Golden Mille Tower and Golden Mille Complex) located along the north side of the CCL alignment. Except for the Plaza which is founded on a mixture of reinforced concrete and steel piles, all the others buildings are founded on steel piles (to Old Alluvium).

2.1.1 Remediation of Partially Completed Excavation

Figure 2.3 shows a more detailed plan view of contract C824, west of the TSA shaft. The MFISH project analyzed the state of construction immediately after the collapse of Nicoll Highway in April 2004.

Segment A-B: has a length of approximately 400 meters; this segment corresponds to 372 meters of subway line and an approximately 40 meter portion of Nicoll Highway Station;
Segment B-C: corresponds to approximately 94 meters of the Nicoll Highway Station;
Segment C-D: corresponds to approximately 152 meters of the Nicoll Highway Station;
Segment D-E: corresponds to approximately 250 meters of the Nicoll Highway Station and 90 meters of regular cut and cover portion;
Segment E-F: corresponds to the collapse zone.

The entire process involved in this project is mainly divided in 4 different and consecutive activities: excavation, pouring of lean concrete at the lowest level of excavation ("Base slab"), reinforced concrete for the station/tunnel boxes and backfilling. Table 2.1 describes the state of the construction based on the proposed activities and segments, and on the information provided with the COI Report (COI, 2005).

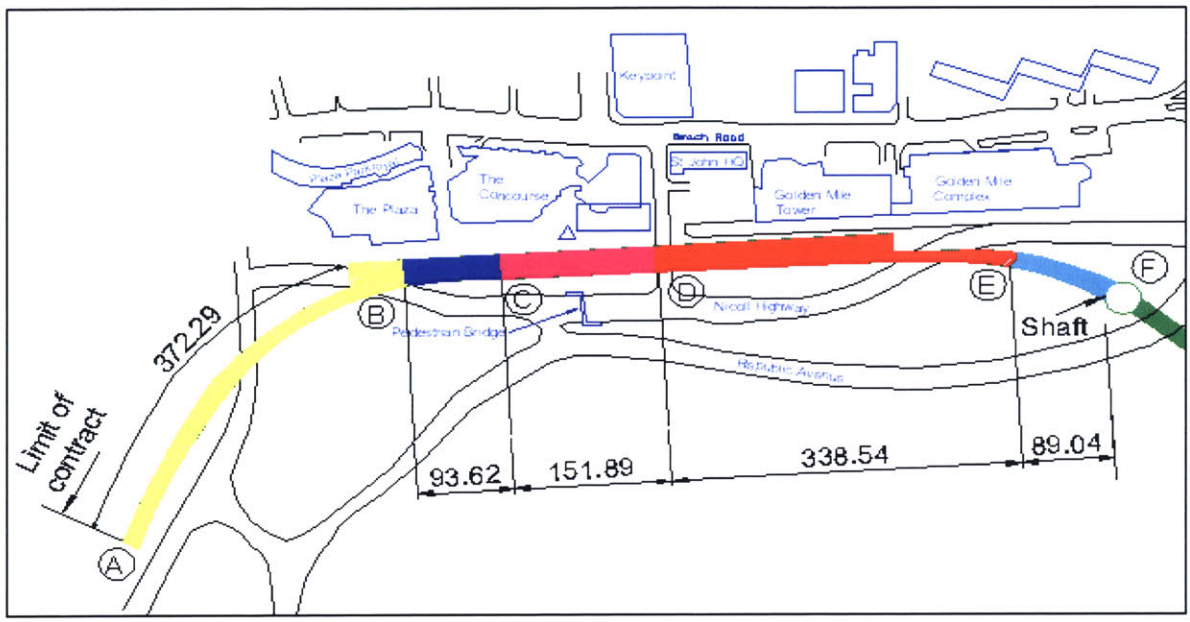

Figure 2.3- Unfinished segments of contract C824

(MFISH, 2006)

Segment	Excavation	Base slab	R/C Works	Back fill
AB	√	√	√	50%
BC	√	√		
CD	√			
DE	50%			

Table 2.1- State of construction of unfinished segments

(MFISH,2006)

A team of MIT students have considered possible methods for completing section C824 of the Circle Line as part of their MEng program. Their final project report (MFISH, 2006) considers two alternatives:1) retrofit/remediation of the partially excavated tunnel using the original alignment, 2)new tunnel construction (alternative alignment).

For option 1, performance of the excavation support system of section K represents one of the key element for reuse of the existing alignment.

The project team identified a series of constrains affecting construction of section K:

- The soil profile is mainly characterized by soft marine clay which manifests high driving forces (active pressures) and low undrained shear.
- The section is located adjacent to existing structures and therefore, further excavation can only be permitted if ground movements are strictly controlled.
- The soil behind the excavation it is not in a "at rest" state of stress and it has already experienced a load.
- The diaphragm wall has already experienced significant stressing during the original excavation (to the 6^{th} level).
- The existing diaphragm wall can only be modified by constructing a second wall in parallel and providing shear connections between the two walls. This is an expensive option.
- The JGP slab below foundation level of the excavation can not be easily modified due to the limited working space.

The purpose of this thesis is to investigate the impact that a new remedial solution can have for section Type K in terms of diaphragm wall displacement, bending moment and strut loads.

The proposed solution consists of the partial reinforcement of the lower marine clay outside the excavation using a soilcrete, jet grout raft. The active force on the bracing system as drawn in Figure 2.4, and has a much higher undrained strength and hence, transmits less stress to the wall. This solution, if applicable, permits a considerable advantage in terms of impact on the structure; in fact it is only necessary to grout on the external side of the excavation without acting directly on the existing wall.

The solution proposed has a lot of advantages; first of all it permits works to be done around buried active utilities without creating a lot of interruption in the installation even considering that the area is economically very active.

Furthermore, ground improvement (Deep Soil Mixing or Jet Grouting) is operatively much faster than other alternative methods even though it is not possible to proceed with the excavation before the setup has reached its design strength.

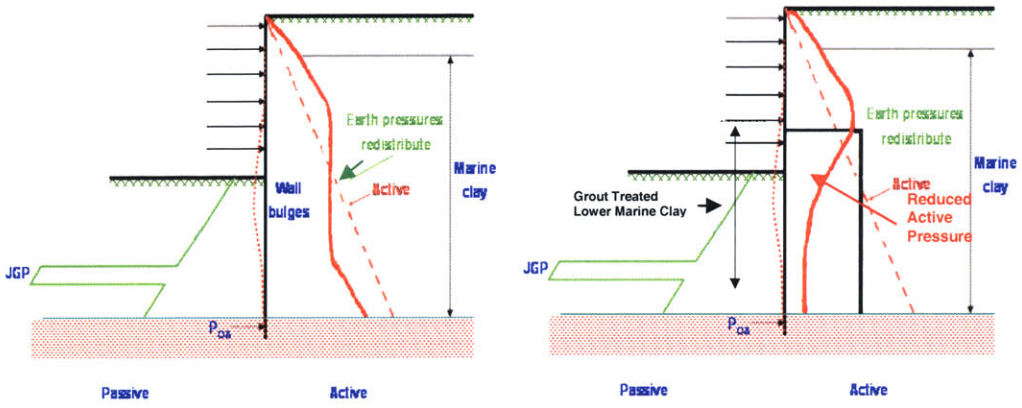

a) Original Design **b) Remedial Solution**

Figure 2.4- Basic Concept for External Grouting Solution

However, even if the proposed remedial performs as expected there is always uncertainty concerning the structural condition of the existing diaphragm wall panels and this will require careful monitoring during all subsequent construction phases.

The aim of this thesis is to provide, with sufficient details, recommendations for the application of this solution, both in terms of design, with the aid of finite element modeling and its accurate interpretation, and in terms of the practical application of the solution itself, with suggestions on the best ground improvement method suitable for the specific conditions of the site and of the project.

3. SITE CHARACTERIZATION AND SOIL CONDITIONS

The location of the site in this study is on the west bank of the Kallang River, between Beach Road and Nicoll Highway, area that was subjected to a first reclamation in the 1930's and 1940's, and to a further one in the 1970's (Whittle, Davies, 2006).

The entire alignment of the C824 traverses through a mixed-soil profile consisting of a layer of granular fill, extending for about 4.5-5.0 m, underlain by 30-35 m of soil of marine, alluvial, littoral, and estuarine origins, dated for the most part in the Holocene period (Tan et al.,2002) and main member of the Kallang Formation; underlying these clay units, a deposit Old Alluvium (OA) is present, dated back to the early Pleistocene (Pitts, 1983, 1984). Figure 3.1 shows the soil profile in relation to the excavation.

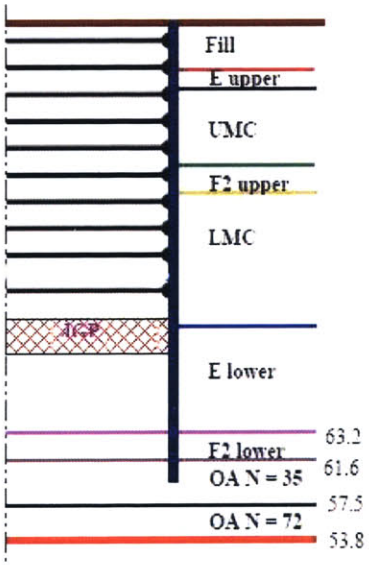

Figure 3.1- Uniform soil profile for C824

The Kallang Formation, which covers much of the coastal and immediate offshore area of Singapore, extending for about one quarter of Singapore Island (Pitts, 1992), consists of two

main layers typically referred as Upper and Lower Marine Clay (UMC, LMC) dated approximately 10,000 and 120,000 years ago respectively (Bird et al., 2003). During the Little Ice Age (10,000 to 12,000 years ago) the sea level dropped and this probably caused the top part of the lower marine clay to be exposed, desiccated and weathered (Lee et al.,2005). The marine clay formation has a thickness variable along the Singapore coastal area; it is usually between 10-15 m near the estuaries but in some other location it can also be around 40 m thick (Tan et al., 2002).

Laboratory tests confirmed the marine clays to be of low overconsolidation ratio (OCR), consistent with the recent reclamation previously cited. In specific, the Upper Marine Clay has an OCR between 1.2 and 1.5 while the Lower Marine Clay is normally or slightly underconsolidated (Whittle, Davies, 2006)

Surface settlement monitoring data show settlements up to 50 mm/yr at the site, suggesting the possibility of on-going consolidation almost 30 years after the last stage of local land reclamation.

The Upper Marine Clay is usually classified as very soft to medium stiff with an undrained shear strength ranging from 10 to 30 kPa; marine or organic materials are often found in this layer.

The Lower Marine Clay, with an undrained shear strength varying from 30 to 50 kPa, is less homogeneous, with occasional sand and peaty clay layers.

In particular for this project, there were three main sources to estimate the undrained shear strength of the Marine Clay and they are respectively: results from undrained triaxial shear tests (CIU test, K_0=1.0), data obtained from field vane shear tests and continuous piezocone penetration resistance data (CPT). Results from CIU tests were mainly used to estimate drained effective parameters for the Marine Clay(c'=0 kPa and Φ'=22°-24°) while data from field vane tests showed a significant scatter and in some cases they were producing very low values of undrained shear strength.

Results of the piezocone tests (CPTUs) are generally more reliable especially for this soil profile. The q_c values have been converted to strengths using the empirical correction factor, N_{kT}, in the following relation:

$$s_u = \frac{(q_T - \sigma_{v0})}{N_{kT}}$$

where

q_T is the measured cone resistance and

σ_{v0} is the total overburden pressure.

The various experts contributing to the COI assumed a N_{kT}=12-14. A N_{kT} value of 14 gives good agreement with piezocone profiles obtained in the site of the project for both the Upper and Lower Marine Clay (Whittle and Davies,2006).

For normally consolidated Marine Clay, a undrained shear strength ratio s_u/σ'_{v0}=0.21 (Tan et al., 2003, for direct simple shear mode) well agrees with piezocone data for Upper Marine Clay. For the Lower Marine Clay the interpreted value for su is about 10 kPa less than the predicted one for normally consolidated clay at elevation 75 m RL; this can be explained by the fact that the Lower Marine Clay is underconsolidated locally and also that the undrained shear strength might be underestimated using N_{kT}=14 for depth higher than 75 m RL. At the same time this assumption gives good consistency at more shallow depth and therefore there is no need to refine the selection of N_{kT} (Whittle and Davies, 2006). Figure 3.2 illustrates the best estimate for undrained shear strength done by Whittle and Davies (2006) and adopted in this thesis.

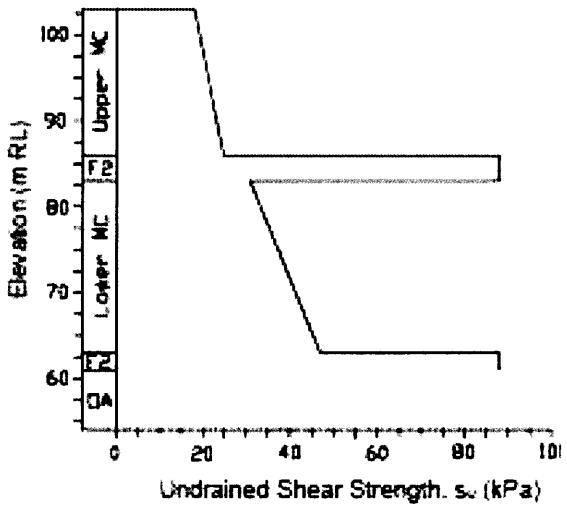

Figure 3.2- Undrained shear strength profile of Marine Clay

(Whittle and Davies, 2006)

Between the lower Kallang layer and the Old Alluvium an alternation of fluvial (F) dense sandy silt and estuarine (E) clay is present, formed during periods when the sea level was more than 25 m below its present level (Bird et al., 2003), and widely considered as desiccated crust of the lower marine clay.

Most of the Old Alluvium is classified as very dense silty sands to very stiff to hard silty clay. SPT blowcount varies with depth from N= 10-20 bpf (blows/300mm) to N>100 bpf. In the interpretation of the physical properties of the Old Alluvium an average SPT blowcount value N>30 bpf is considered, being this range accurate to provide enough toe resistance for the diaphragm wall (Whittle, Davies, 2006).
Whittle and Davies investigated on the role of pore pressure development in the Old Alluvium layer while proceeding with the excavation and they conclude that very little migration occurs within the time frame of the excavation and the assumption of undrained shearing conditions in the weathered OA is more than reasonable. The excess pore pressure generating in the Old Alluvium while proceeding with the excavation is governed by the following equation:

$$\Delta u=B\Delta\sigma_3+AB(\Delta\sigma_1-\Delta\sigma_3) \qquad (3\text{-}1)$$

where A and B are known as Skempton parameters and $\Delta\sigma_1$ and $\Delta\sigma_3$ are the changes in total principal stresses due to the excavation. Field data from the very few piezometers installed beneath the excavation in the weathered OA are consistent with finite element simulations in the assumptions of undrained shear conditions (Whittle and Davies, 2006).

The groundwater table in the fill ranges from 100.0mRL to 100.5mRL with an excess piezometric total head of 102m-103m below the Marine Clay..
Through all the analysis that will be carried out a constant hydraulic total head of 102.9m is assumed.

4. PROJECT DESCRIPTION AND MODELLING

The construction of the mining tunnels in contract C824 involves 30-35 m deep cut-and-cover excavations supported by diaphragm walls with cross-lot bracing. The excavation width varies from 20 m to 31 m.

The excavation is temporarily supported by 0.8 m to 1 m-thick diaphragm wall installed in Old Alluvium. The walls are supported by a strutted system comprising 9 to 10 levels of steel struts with a horizontal spacing of 4 m to 6 m and a vertical spacing from 3 to 3.5 m; king posts piles are previously driven to provide vertical supporting for the cross-lot struts. Dependently on the location one or two slabs of Jet Grout Piles (JGP) are installed to minimize deflection and control ground movement during the excavation process. A series of bored piles is used to support the final tunnels.

The construction sequence for a typical cross section adopted in the project is graphically described in Figure 4.1.

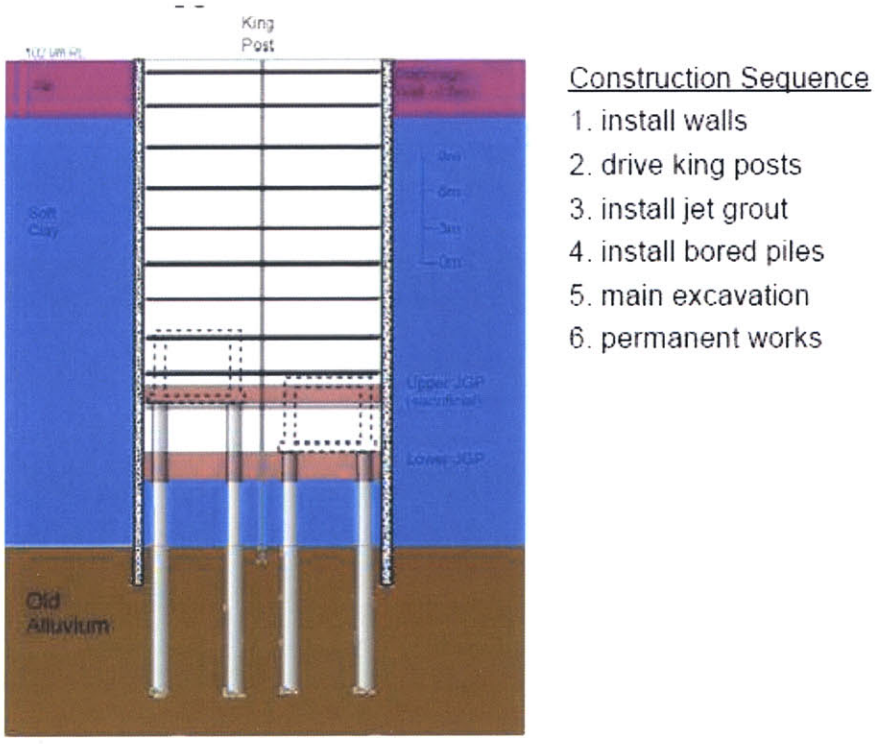

Figure 4.1- Construction Sequence for C824

(Davies et al.,2006)

As previously described, this study is focused on a specific section of contract C824 which corresponds to the Cross Over Box portion of the alignment close to Nicoll Highway Station, referred to as section Type K.

Type K is the widest section in the alignment and was subjected to a series of construction delays due to excessive wall deflections prior to the April 2004 collapse at section M3/M2. At the time of the collapse section type K was excavated to the 6^{th} level of excavation with 5 levels of struts installed.
The section was backfilled after the collapse.

Section type K, Figure 4.2, is 31.6 m deep and approximately 31 m wide. A concrete cast in place diaphragm wall, part of the temporary works, is designed to support the sides of the excavation; 9 levels of internal struts and interlocking Jet Grout Piles (JGP) which form a continuous 1.5 m-thick slab at the bottom of the excavation and whose main is to brace the toe of the wall, to reduce bending moments and control lateral wall deflection, consist the original excavation retaining system.

The diaphragm wall is 0.8 m thick and extends from ground surface down to a depth of 45 m embedded in the Old Alluvium for a total length of about 3.7 m.
The JGP is 1.5m thick extending from the bottom of excavation while the internal strutting system comprised of steel H sections, pre-loaded at the time of installation. The horizontal spacing between rows of struts was 4 m.. For the purpose of this study, the soil profile (Table 4.4) is considered the same on both the sides of the excavation.

Table 4.1 describes the strutting system according to the original design. Since the excavation was backfilled, any proposed remedial solution can introduce an improved design of the strutting system (MFISH,2006).Table 4.2 summarizes the revised strut system.

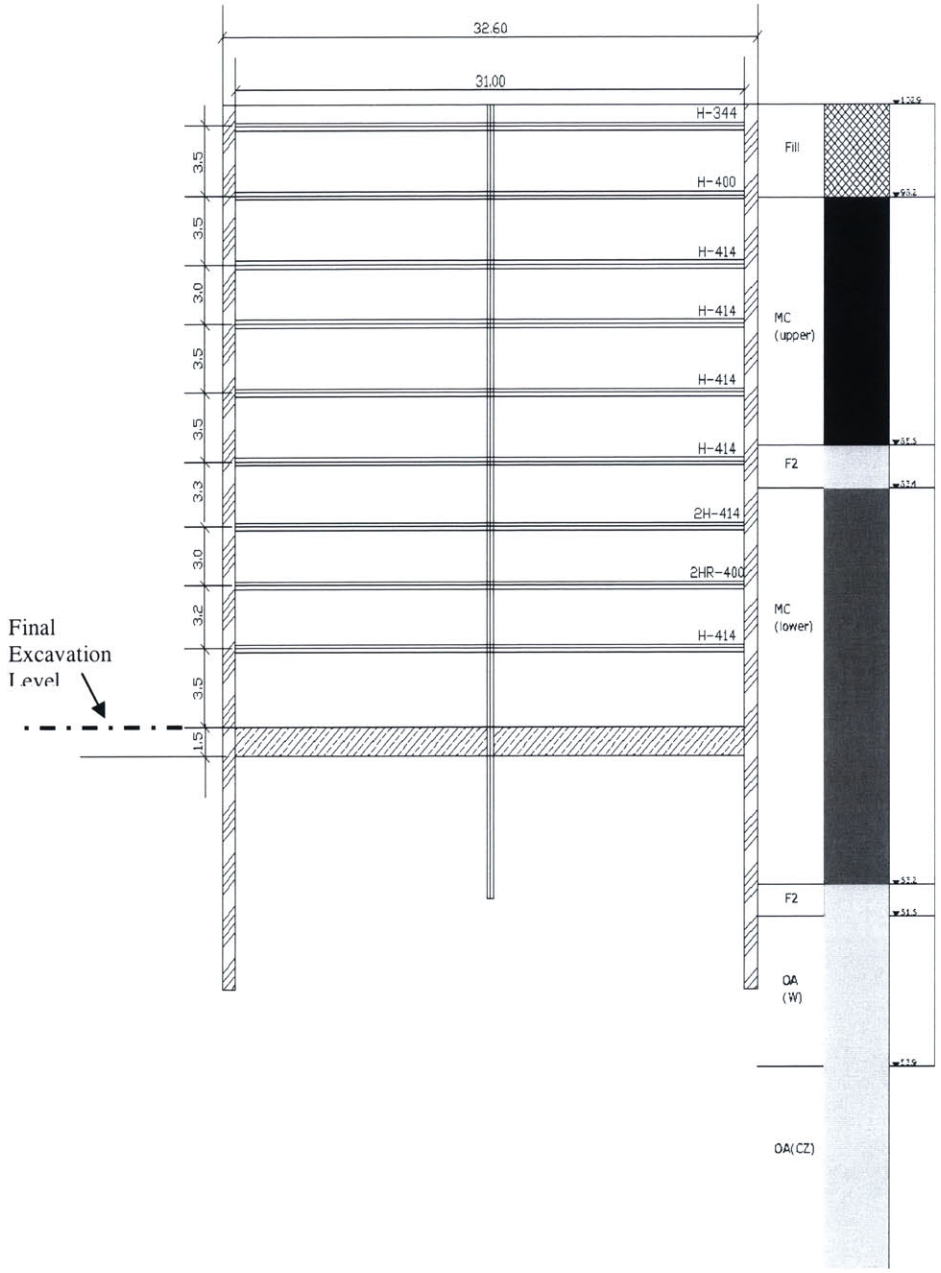

Figure 4.2- Detail of typical cross section K, original design

(MFISH,2006)

Table 4.1- Details of Internal Bracing System, Original Design

Strut Level	Dimensions (mm)	EA (kN/m)*10^6	Installation Depth (m)	Preload (kN/m)	F_{max} (kN)
1	H344	0.9	RL-1.1	150	825
2	H400	1.15	RL-4.6	200	975
3	H414	1.55	RL-8.1	450	1200
4	H414	1.55	RL-11.6	600	1200
5	H414	1.55	RL-15.1	600	1200
6	H414	1.55	RL-18.6	600	1200
7	2H414	3.1	RL-21.9	750	2400
8	2HR400	2.1	RL-24.9	600	1950
9	H414	1.55	RL-28.1	400	1200

Note : Flexural stiffness of diaphragm wall=8.36*10^5 kN-m^2/m, axial stiffness= 2.24*10^7kN/m,maximum bending moment= 2.3*10^3 kN-m/m

In the original design, after the diaphragm wall installation and the creation of the JGP raft, the excavation was scheduled for completion in 10 stages. In the model adopted no changes are considered in the installed JGP layer at the bottom of the excavation; in fact as previously said, it is practically very difficult to modify this raft due to the limited working space available. Details of the construction sequence are listed in Table 4.3.

Table 4.2- Details of Internal Bracing System, Revised Design (MFISH,2006)

Strut Level	Dimensions (mm)	EA (kN/m)*10^6	Installation Depth (m)	Preload (kN/m)	F_{max} (kN)
1	H344	0.9	RL-1.1	200	825
2	H400	1.15	RL-4.6	200	975
3	HEA260	1.788	RL-8.1	600	1800
4	HEA260	1.788	RL-11.6	600	1800
5	HEA280	2	RL-15.1	600	2140
6	HEA280	2	RL-18.6	600	2140
7	2HEA260	3.576	RL-21.9	600	3600
8	2HEA260	3.576	RL-24.9	600	3600
9	HEA260	1.788	RL-28.1	400	1800

Table 4.3- Construction Sequence

Stage	Construction Activities
1	Diaphragm wall installation
2	Distributed load activation
3	JGP slab installation
4	Excavate to RL-2.1m
5	Install and preload 1st level of strut
6	Excavate to RL-5.6m
7	Install and preload 2nd level of strut
8	Excavate to RL-9.1m
9	Install and preload 3rd level of strut
10	Excavate to RL-12.6m
11	Install and preload 4th level of strut
12	Excavate to RL-16.1m
13	Install and preload 5th level of strut
14	Excavate to RL-19.6m
15	Install and preload 6th level of strut
16	Excavate to RL-22.9m
17	Install and preload 7th level of strut
18	Excavate to RL-25.9m
19	Install and preload 8th level of strut
20	Excavate to RL-29.1m
21	Install and preload 9th level of strut
22	Excavate to RL-31.6m

4.1 Finite Element Model for Section Type K

This section summarizes the key features of a 2D finite element model that has been developed to simulate the excavation support system of type K. The calculations are performed using the *PLAXIS* program (v. 8.2, www.plaxis.nl).

4.1.1 Geometry

The typical cross section with the correspondent mesh used as geometry input for the problem in this study is evidenced in Figure 4.3. The soil profile and the structural elements are assumed to be identical on both side of the excavation and symmetrical to the center line of the excavation . Hence, due to the vertical symmetry present, only the left half of the excavation has been modeled and every soil layer is therefore horizontally modeled.

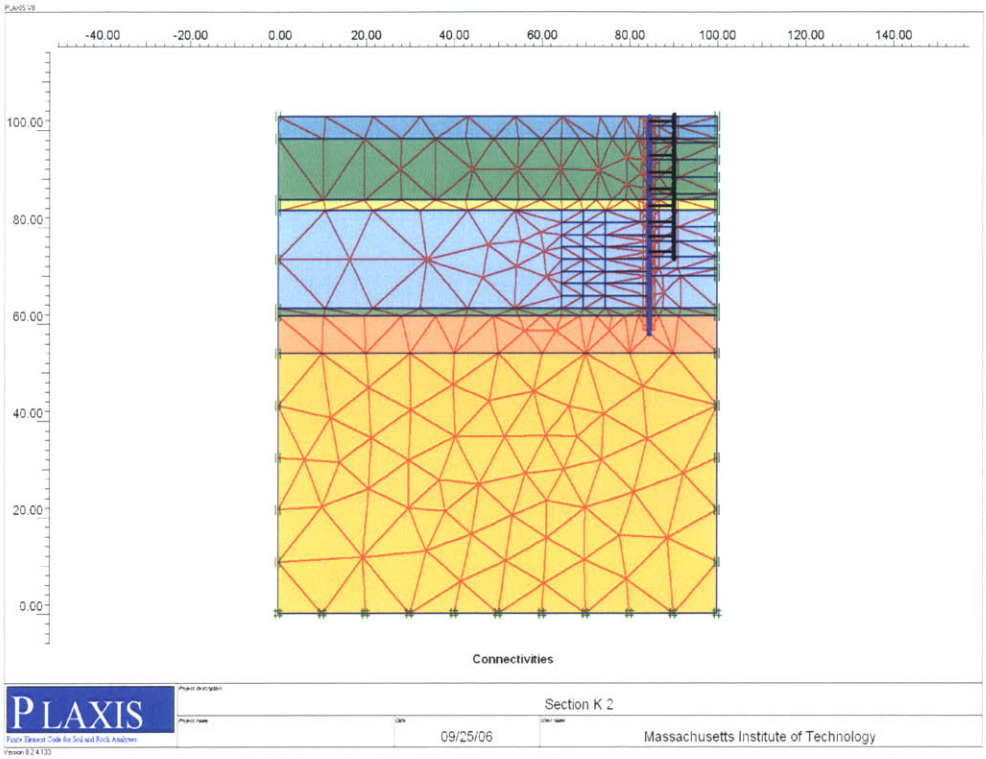

Figure 4.3-Uniform soil profile with correspondent mesh used in the analysis

Boundary conditions are created with the option *Standard Fixities*, generating automatically full fixities at the bottom and vertical rollers at the vertical sides.

The retaining diaphragm walls are modeled using 2D *plate* elements. Plates are structural objects suitable for elements with significant flexural rigidity. This class of geometry input well model the behavior of two-dimensional elements structures extending on the z-direction and having a load applied or induced in a direction normal to the mean axis (Figure 4.4) such as walls, plates or shells.

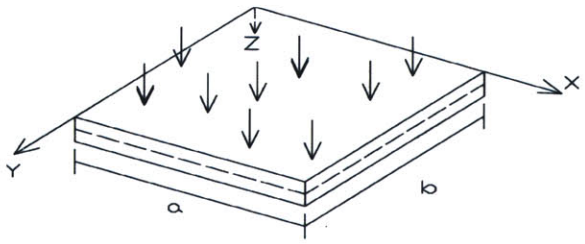

Figure 4.4-Plate model

In particular in the program input of the flexural rigidity EI and the axial stiffness EA are requested. Figure 4.5 shows how the axial and flexural stiffness are computed for this specific case.

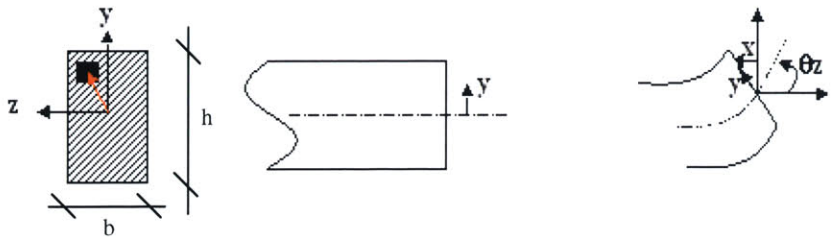

Figure 4.5-Computed axial and flexural stiffness for diaphragm wall

In particular:

$$EA = E \cdot b \cdot h$$

$$EI = E \cdot \frac{b \cdot h^3}{12} \cdot 0.7$$ [1]

With E=2.8*10^7 kN/m^2 (average Young's modulus for reinforced concrete), b=0.8 m (thickness of the diaphragm wall) and h=1 m^2.

M_p value for plastic capacity of the diaphragm wall is computed based on average reinforcement used in a adjacent sections.

From these two parameters an equivalent wall thickness is calculated in *PLAXIS* from the equation

$$d_{eq} = \sqrt{12 \frac{EI}{EA}} \qquad (4\text{-}1)$$

The cross-lot bracing is modelled using *fixed-end anchors*, comprising one-node spring with a constant stiffness EA fixedly connected to the soil mass and properly pre-stressed at each stage of excavation. The model also enables input of the maximum allowable compressive stress for

[1] 70 % of the total flexural stiffness has been considered in the model.
[2] Values are computed per linear meter of diaphragm wall.

each strut coherently with the values in Table 4.1 and 4.2; no tensile capacity is given to the struts in the model.

A distributed load of 20 kPa is entered in the geometry to model potential surcharge on the ground surface (e.g. due to material storage, heavy construction vehicles, etc.) close to the excavation and extending for 20 m. The load in the construction process is added in the stage following the installation of the wall.

4.1.2 Material Constitutive Behavior

Material properties that are used for the geometry input are identified as part of the field and laboratory investigations performed in the site and described in Chapter 3.
All the geotechnical design parameters (unit weights, K_0, hydraulic conductivity, elastic stiffness parameters and Mohr-Coulomb shear strength parameters) for the typical soil profile considered are summarized in Table 4.4 after Whittle and Davies, 2006.
The JGP has been modeled as a cluster with properties shown in Table 4.4 as well and its installation is simply done substituting the cluster representing the lower marine clay with the new one correspondent to the jet grout and then activating the cluster itself.

Table 4.4- Soil Profile

Soil Layer	RL (m)	γ (kN/m^3)	su (kPa)	Φ'	G (Mpa)	ν'	k (m/day)	K_0	H (m)
Fill	102.9	19	0	30	4	0.25	0.086	0.5	102.9
Upper MC	98.2	16	20 25	-	3	0.25	$8.6*10^{-5}$	0.7	102.9
F2 Clay	85.6	19	88	-	11.7	0.25	$8.6*10^{-5}$	0.7	102.9
Lower MC	83.4	16.8	31 47	-	5.2	0.25	$8.6*10^{-5}$	0.7	102.9
F2 Clay	63.2	20	88	-	11.7	0.25	$8.6*10^{-5}$	0.7	102.9
OA Weathered	61.6	20	100	-	40	0.25	$8.6*10^{-4}$	0.7	102.9
OACompetent	53.9		500	-	67	0.25	$8.6*10^{-5}$	1.0	102.9
JGP		16	300	-	108	0.15	$8.6*10^{-5}$	1.0	102.9

Note : G: elastic shear modulus $G = \frac{E}{2(1+\nu')}$; v: Poisson's Ratio, k: hydraulic conductivity, H: piezometric head.

PLAXIS offers a range of material constitutive model to represent soil stress-strain-strength interaction (Hardening-Soil, Soft-Soil, etc.). They consist of a series of mathematical equations describing the mechanical (stress-strain-strength) properties of the soil.

The choice for a particular model is led by the amount of information available from field and laboratory investigations.

The selection of constitutive model is conditioned by the amount of data available and by the aspects of behaviour needed to achieve realistic simulation.

In general most constitutive models used in geomechanics are based on the concept of plasticity. For the analysis here carried out, all soils are modelled as simple linear elastic, perfectly plastic isotropic materials obeying Mohr-Coulomb yield criterion. Mohr-Coulomb is an elastic-perfectly-plastic (EPP) model with a fixed yield surface independent of plastic straining (Figure 4.6). In this model for every stress state, that in a ε-σ plot are represented by a point within the yield surface, the Hooke's law governs and all strains are reversible.

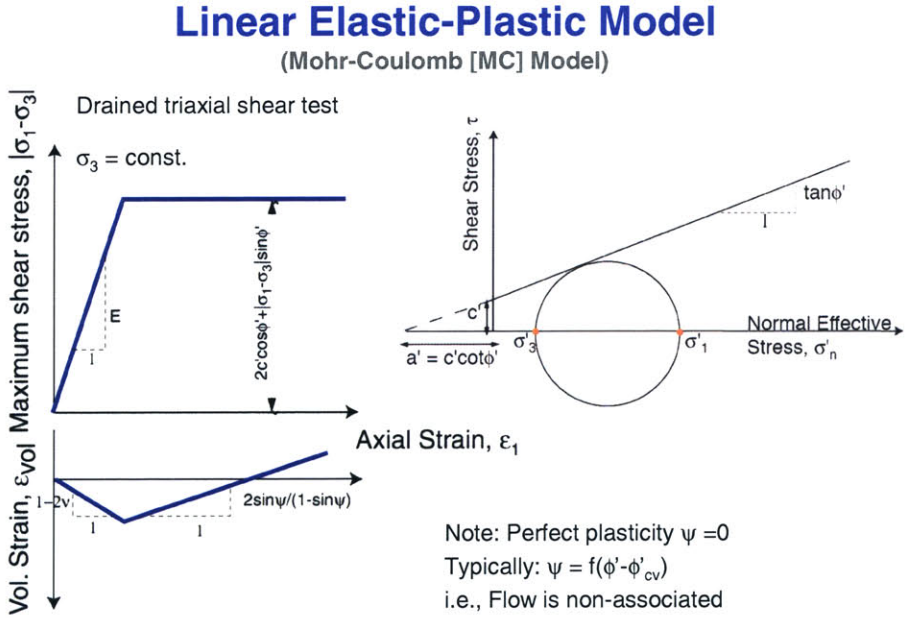

Figure 4.6-Elastic Perfectly-Plastic Model

The model requires five input parameters, E' (or G) and ν' for soil elasticity; Φ' and c' for shear strength , and K_0-values to generate the initial horizontal stress state.

The undrained shear strength of the clay can be represented either using A) effective stress-strength parameters (c' and Φ', respectively apparent cohesion and internal friction angle) or B) undrained shear strengths ($c' \Rightarrow s_u; \Phi'=0$); this two approaches are referred as Method A and B in the COI report (Whittle and Davies,2006).

During undrained shearing in EPP model, there is no change of mean effective stress and in a p,p'-q stress-path space, for undrained triaxial compression tests with Ds3=0, A=0.33 while all undrained plane strain shear modes are characterized by A=0.5 (Figure 4.7) (Whittle and Davies,2006)

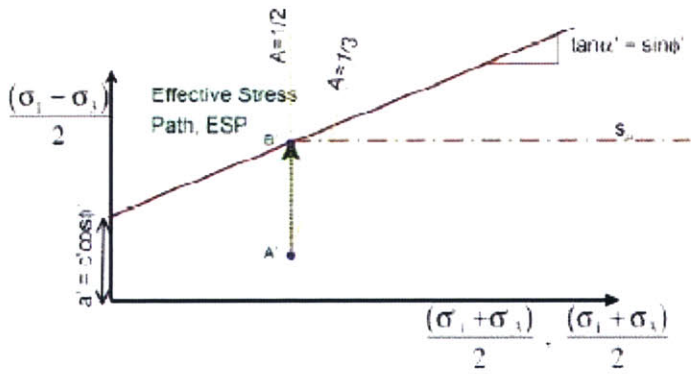

Figure 4.7-Elastic stress path for undrained plane strain shearing using Mohr-Coulomb soil model

(Whittle and Davies, 2006)

Assuming initial K_0 conditions in the ground, the equation expressing the undrained shear strength ratio is the following:

$$s_u/\sigma'_{v0}=(c'/\sigma'_{v0})\cos\Phi'+1/2(1+K_0)\sin\Phi' \qquad (4\text{-}2)$$

Comparing values for undrained shear strength ratio obtained from equation (4-2) with widely used empirical correlations relating the s_u/σ'_{v0} ratio to the overconsolidation ration OCR

(SHANSEP; Ladd and Foott, 1974), it is evident that Method A with input of effective stress-strength parameters overestimates the undrained shear strength of the clay for very low OCR (Figure 4.8) and this obviously determines underestimation of the stress acting on the structural elements obtained from finite element simulation. Direct input of undrained parameters (Method B) is the most reliable way of applying EPP Mohr- Coulomb model for contract C824 (Whittle and Davies, 2006).

Initial pore pressure is hydrostatic with the groundwater table located at ground surface (102.9 m).

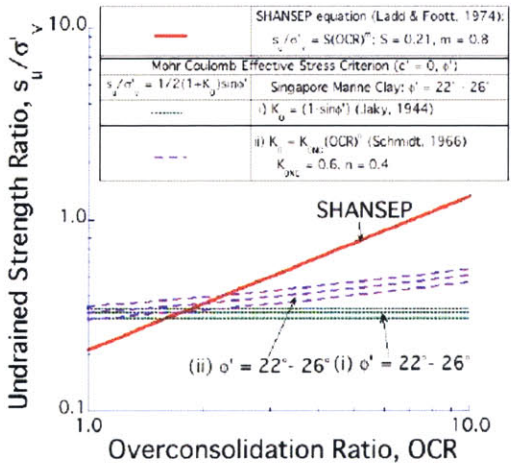

Figure 4.8- Comparison of the undrained stenght ratio for the Marine Clay with empirical correlations based on SHANSEP

(Whittle and Davies, 2006)

5. PARAMETRIC STUDY

5.1 Outline

Section Type K is considered by the Land Transportation Authority as one of the most critical among the different types in the project; it is located close to major buildings and utilities in the XOB portion of the contract at the joint with CC2.

Technical details on the original design of this section are presented in Chapter 4.

Excavation at Type K started in June 2003 and stopped at the 3rd level in mid July 2003 due to a "slope failure" incident. It resumed two months later, until the excavation reached the 6th level when an inclinometer located close to the north side of the wall reached the trigger level in early December 2003 and some cracks were noticed on the wall. Thereafter, the excavation was closely monitored until the moment that the inclinometer exceeded the design level in January 2004 and the excavation was immediately blocked. At this point a series of measure were taken to control the extensive deflection the panels were experiencing- reducing strut spacing, adding more struts-and a series of design back analysis were carried out (see Chapter 4 for details).

By 25 March 2004, the maximum deflection at Type K as recorded by the inclinometer above mentioned and the design level was exceed of 422 mm.

Some people involved in the design and back analysis of this section stated that a failure was likely to occur if the excavation would have exceed the depth of 25 m.

While a new series of back analysis were developed before start again with the excavation, on 20 April 2004 a major collapse happened in correspondence of section Type M, the trench in section Type K was backfilled and the attention moved on the collapsed area.

A series of finite-element analysis have been carried out to evaluate the effectiveness of external ground improvement on the excavation performance for section Type K previously described.

As a first estimation of the effects of the treatment , the finite element model the phases of the excavation as in Table 4.3 and used a revised set of struts as in Table 4.2, previously discussed.

The primary variables considered are the thickness of the treatment zone h which corresponds to the height of the jet grout (or deep mix) columns of improved soil, the percentile plan coverage

of the treatment behind the wall, the lateral extension of the treated soil Δ (Figure 5.1) behind the diaphragm wall, the treatment strength ratio $N = \frac{s_{uT}}{s_{u0}}$, where s_{uT} is the design strength of the soilcrete (nominally at 28-days) and s_{u0}, the undrained shear strength of the soft marine clay.

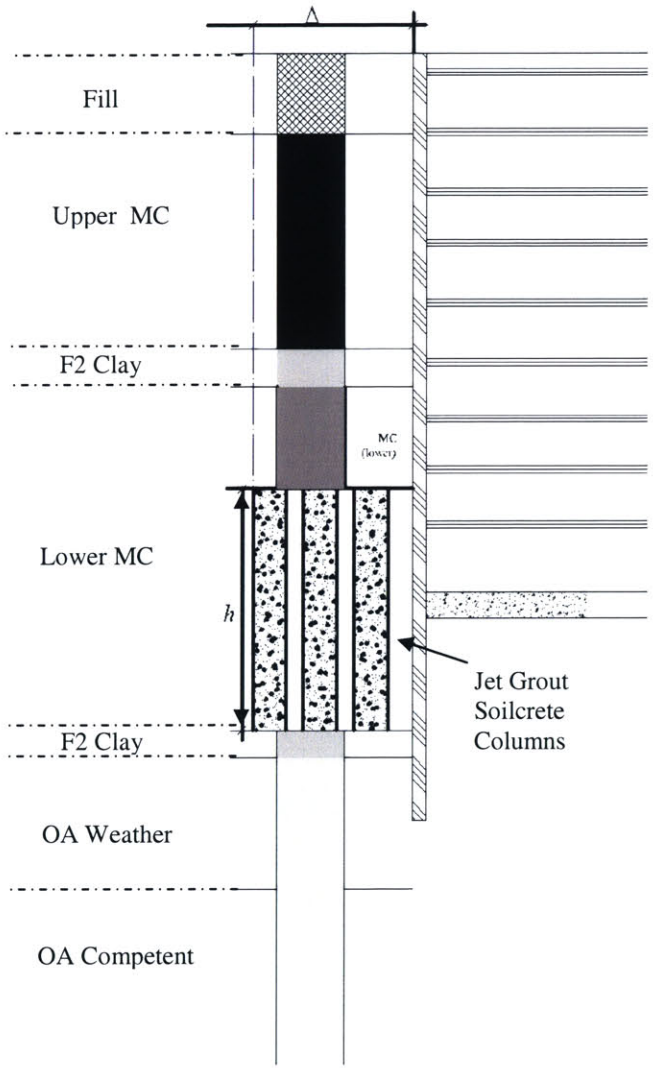

a) vertical section

b) plan view

Figure 5.1-Primary variables analyzed

A wide range of conditions are analyzed varying the primary variables mentioned above and they are summarized in Table 5.1.

Table 5.1- Conditions Analyzed

h (m)	*N*	% coverage	Δ (m)
8,10,13,15, 18,20	1,3,5,7,9	0,30,50,80, 100	10,15, 20

5.2 Effects of Vertical Treatment Thickness *h*

The effects of the proposed external reinforcement solution with the above-mentioned variables are presented, focusing on the maximum wall deflection, wall bending moment and strut loads.

5.2.1 Lateral Wall Deflections

Figures 5.2 to 5.4 show typical predictions of lateral wall deflections for the excavation considered[1] using fixed value of Δ=10 m, N=7.5 and total percentage of plan coverage. Fig. 5.2 compares results for six different values of column height, from 20.2 m, the entire layer of LMC, to about 8 m. Lower values of *h* are not considered since they implies a geometrical discontinuity between the new improved soil and the existent JGP slab inside the excavation. The effect of the height of the grouted columns on the deflected shapes of the wall is immediately apparent: the higher *h*, the lower is the overall deflection along wall at the last stage of excavation (RL

[1] Positive movement refers to movements toward the excavated side

71.3m). The maximum horizontal displacement is reached underneath the bottom of the excavation, at about 6 m from the toe of the wall, except for h=7.6 m where the deflected shape is associated with a point of contraflexure (as for the original design, h=0) in correspondence of the bottom of the excavation and a maximum displacement of about 50 % higher than for the other cases. In this last case there is likely the possibility of the formation of a plastic hinge in open trench.

When the height of the grouted columns is less than 5 m above the bottom of the excavation ($h \leq$ 12.6 m), the effect of the discontinuity between the properties of the LMC and the grouted soil is evidenced by the irregularity of the deflected shapes. However, for $h \geq$ 12.6 m the plot shows little difference in the wall deflection. In fact, with treatment there is a maximum computed wall deflection of about 200 mm which occurs below the final formation at about RL 64 m.

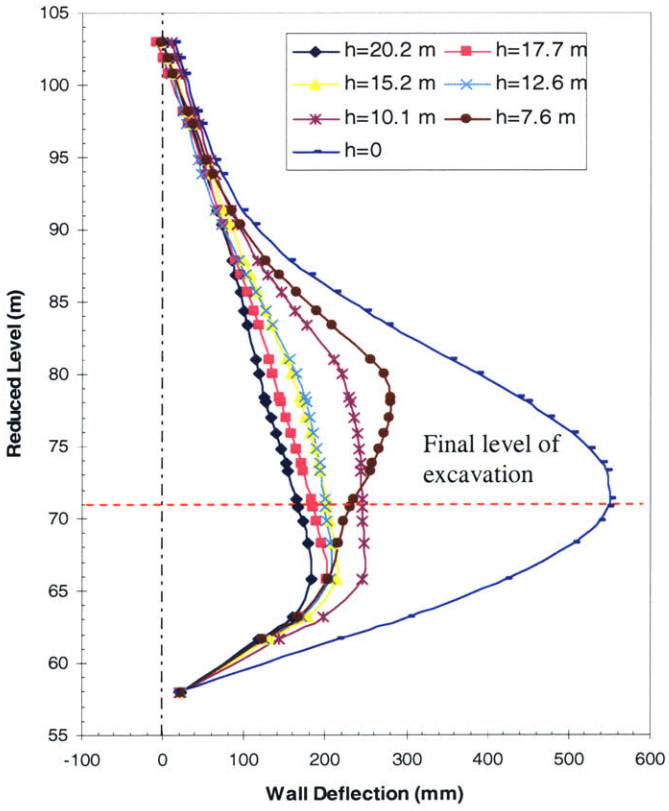

Figure 5.2-Effect of treatment thickness, *h*, on wall deflection for excavation at RL. 71.3 m

The effect of the improved soil in controlling lateral wall deflections during excavation is also clear in Figure 5.3 where comparison of the deflected shapes of the wall as a function of the excavation depth is plotted for a model assuming elastic behavior of the wall with and without treatment. The deflected mode shapes of the wall are plotted for each of the 10 stages of excavation until RL 71.3 m (refer to Table 4.3 for details on steps).

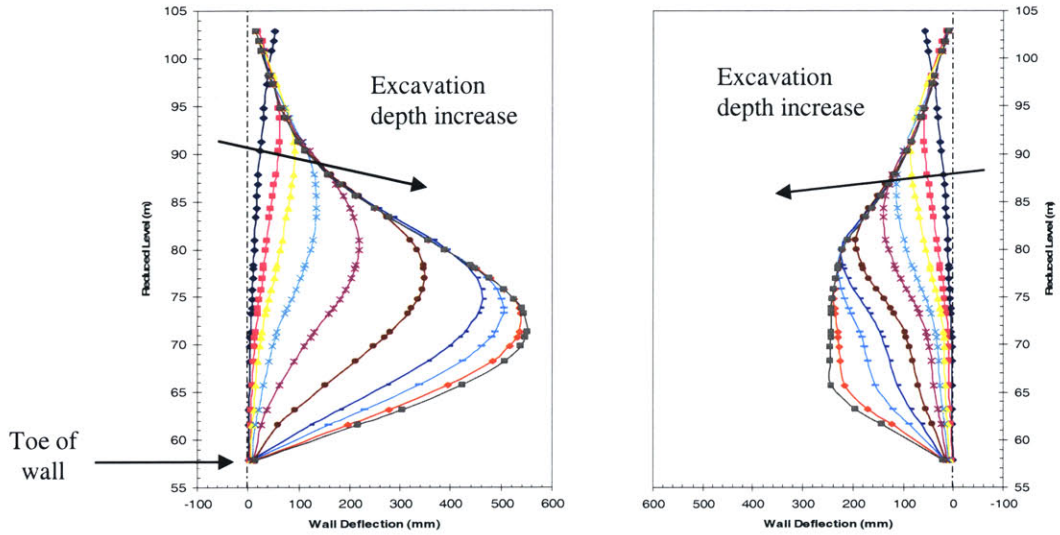

a) fig. left: no treatment, fig. right: h= 10.1 m

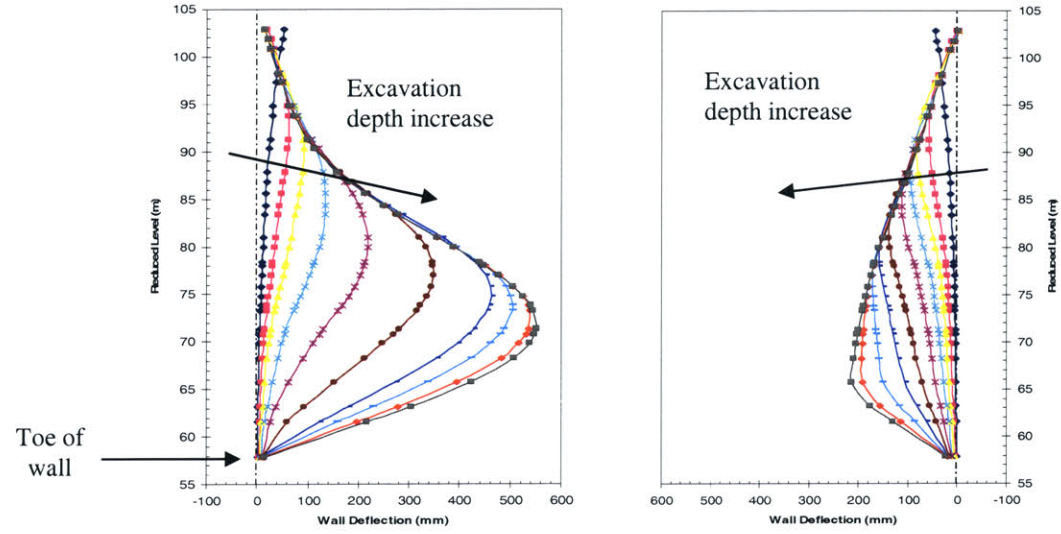

b) fig. left: no treatment, fig. right: h= 15.6 m

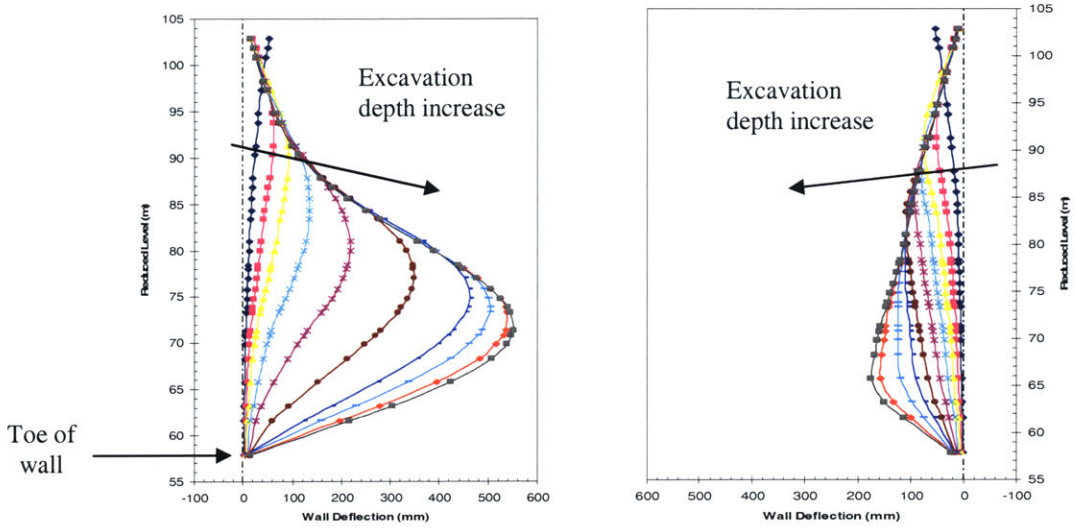

c) fig. left: no treatment, fig. right: h= 20.2 m

Figure 5.3-Comparison of the effects of treatment thickness through excavation stages

For steps 2 to 4 the maximum wall deflection reaches the same magnitude for cases a), b) and c). However from step 5 onwards the untreated excavation exhibit much larger deflection.

At a glance the discontinuity between the LMC and the properties of the improved soil is confirmed in Figure 5.3.a corresponding to h= 10.1 m. The percentile variation of maximum deflection in the improved case is quite constant all over the excavation process and it ranges between 10 to 15 % .

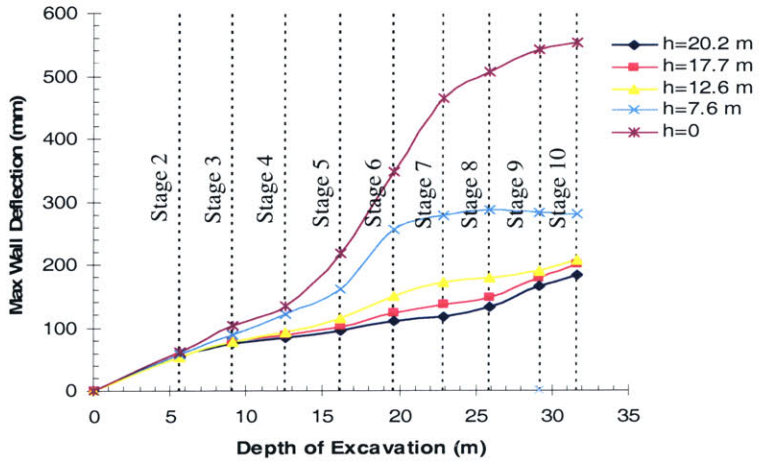

Figure 5.4-Maximum computed horizontal deflection against excavation depth for different h

Observing the trend of the maximum wall deflection plotted against excavation depth (Figure 5.4[2]) , the effect of the intervention starts to be clear at the depth of 12.6 m (4th stage of excavation); here, there is a significant difference between the cases analyzed. For $h \leq 12.6$ m the increment of deflection is higher than for $h \geq 17.7$ m (higher slope of the curve).

5.2.2 Wall Bending Moments

In the analysis in this study carried out, one of the main constraint associated with the solution proposed consists in the fact that it is not possible to modify structurally the diaphragm wall that has been already cast in place.

The evaluation of the bending moment acting on the wall represent therefore one of the main elements that need to be considered.

Figure 5.5 plots the bending moment acting on the wall in the last four stages of excavation, from RL 80 m to RL 71.3 m, for the original case; assuming elastic behavior for the struts and for the wall (in fact, yielding moment of the reinforced diaphragm wall is 2300 kNm/m, refer to Chapter 4 for details) are here assumed in the finite element model. The bending moment is defined as positive when the tension face of the wall is on the excavation side. It is here evident that at stage 7 (RL 80 m) the computed bending moment has well far exceed the bending capacity of the wall and there is likely the formation of two plastic hinges along the wall itself; at elevation RL 88 m, RL 83 m and RL 68 m the bending moment diagram significantly exceed the value of 2300 kNm/m. In particular elevation RL 88 m and RL 83 m, when the excavation reaches the final level at stage 10 (RL 71.3 m), are located in the open trench and the wall is potentially driven in the inner side of the excavation without any support. Significant rotation of the toe of the wall is also evident.

Consequently, it is obvious that part of the efficiency of the solution here proposed is strictly correlated with the control of the flexural behavior of the wall.

[2] Values from Stage 1 are not computed because wall bend as cantilever without support in that phase.

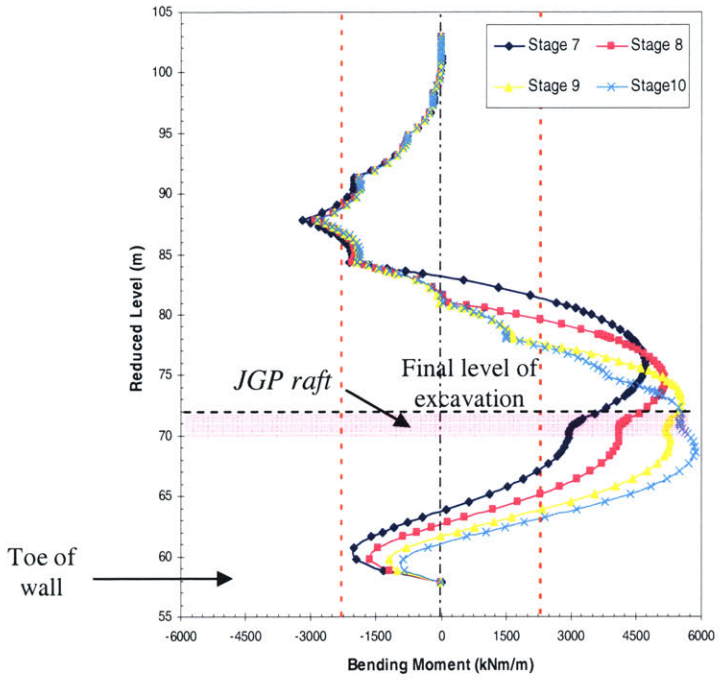

Figure 5.5-Bending moment on diaphragm wall without treatment at last 4 stages of excavation

Figure 5.5 shows results for the computed bending moment as a function of the thickness of treatment *h* through various excavation stages (the same stages and the same scale as Figure 5.4 has been used for easier comparison). The thickness *h* reduces the maximum bending moment in the wall diagram especially in the last stages of excavation. In all the four cases presented the moment curves for each excavation level perfectly coincide until RL 84.3 m (location of the 6th strut) and close to where the LMC layer begin. For *h*=20.2 m (Figure 5.6a) maximum positive moment on the excavation side is reached at level RL 64.5 m, in the LMC and underneath the bottom of the excavation; its value range between 2335 and 2342 kNm/m (just sufficient to cause a plastic hinge). The maximum positive moment value does not change notably with different values of *h*, while a significant increase in the negative moment develop especially for h $\leq$ 10.1 m. It is also evident that lowering the thickness of the treatment determines an increase in the positive bending moment on the upper part of the wall. Referring to figure 5.5.d for example it is clear that the yielding moment of the wall is almost mobilized at 3 elevations potentially generating a collapse mechanism in the wall. When a "plastic hinge" is formed, increasing

rotation at that location would no longer be accompanied by increasing rotational resistance and the wall will be more curved than the soil behind it. Also, when an hinge develops in the wall, considering the toe of the wall as a structural hinge too, the formation of one more plastic hinge will occur in a dynamic mechanism of collapse[3].

The results suggest a minimum thickness $h \geq 12.6$ m necessary to keep a margin of safety in the overall construction process needs.

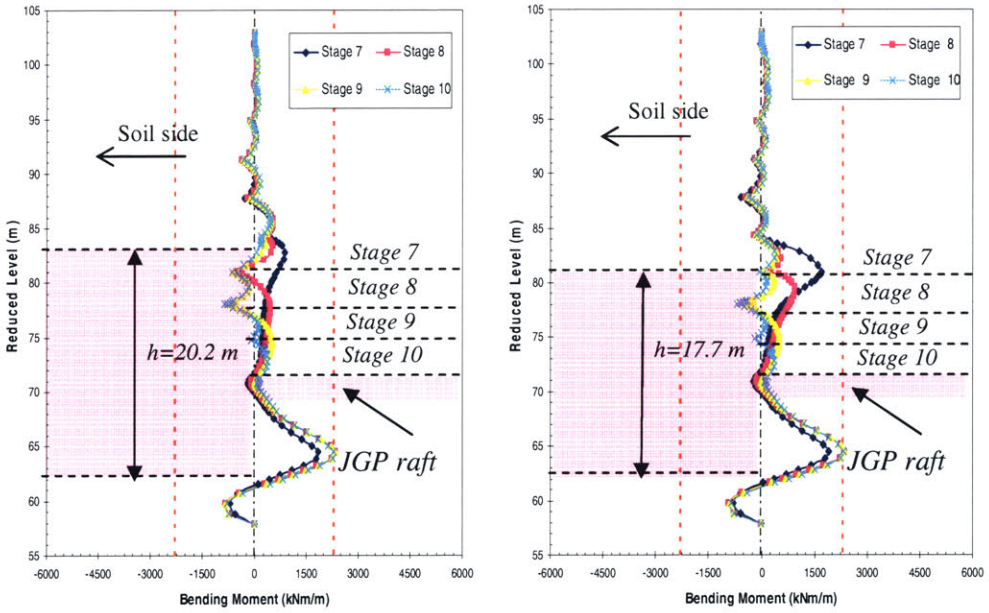

a) h= 20.2 m

b) h= 17.7 m

[3] In the original design, at the 6th level of excavation the diaphragm wall yields in two points and a collapse mechanism develops.

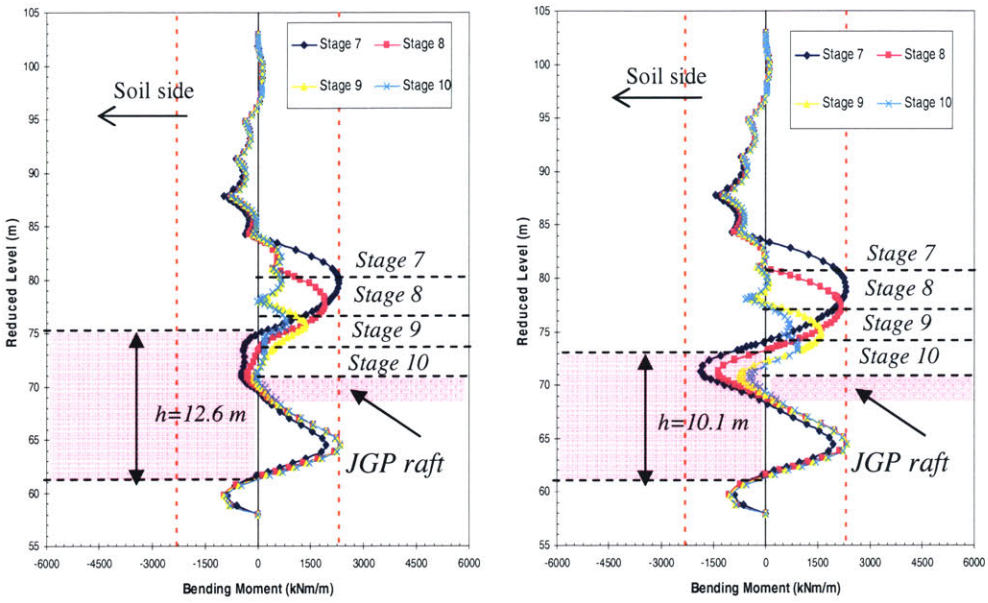

c) h= 12.6 m **d) h= 10.1 m**

Figure 5.6-Computed bending moment acting on the diaphragm wall as function of treatment thickness *h* for stages 7 to 9

5.2.3 Strut Loads

Another important factor affecting the performance of deep excavations are in the strutting system and its behavior throughout the excavation process.

Figure 5.7 to 5.8 described the computed results in term of struts load for the parametric study carried out[4].

Table 5.2- Computed strut loads for different value of thickness of treatment h

Strut \ Stage	1	2	3	4	5	6	7	8	9
1									
2									
3									
4	0.0								
5	200.0								
6	373.1								
7	260.7	200.0							
8	95.0	731.6							
9	141.0	395.7	600.0						
10	18.0	341.6	1157.7						
11	70.5	326.1	727.4	600.0					
12	15.1	200.7	635.3	1572.4					
13	25.6	232.0	616.2	1182.0	600.0				
14	30.6	189.3	416.8	1044.6	2117.0				
15	28.3	199.3	450.3	1023.2	1723.7	600.0			
16	39.4	203.5	393.4	817.9	1628.8	2151.4			
17	37.5	202.5	406.8	855.2	1591.4	1662.6	600.0		
18	28.8	194.8	398.1	820.5	1467.1	1502.5	1690.2		
19	29.3	193.4	396.3	827.6	1496.0	1513.8	1237.3	600.0	
20	31.1	195.2	398.2	822.8	1452.9	1396.5	1191.1	1653.7	
21	31.6	194.9	397.0	822.6	1459.8	1414.4	1168.6	1422.6	400.0
22	26.6	189.5	390.4	815.7	1450.2	1392.4	1090.1	1462.6	930.5

a) h= 0 m, no treatment

Strut \ Stage	1	2	3	4	5	6	7	8	9
1									
2									
3									
4	0.0								
5	200.0								
6	293.5								
7	181.7	200.0							
8	116.4	740.3							
9	173.9	302.6	600.0						
10	127.3	266.1	894.7						
11	174.2	260.9	467.9	600.0					
12	162.6	229.2	521.2	1249.6					
13	168.8	255.7	509.4	879.6	600.0				
14	162.8	231.7	430.4	869.2	1431.1				
15	158.0	236.4	454.8	855.7	1082.2	600.0			
16	153.2	239.8	448.9	789.4	978.8	881.4			
17	150.4	238.8	453.8	801.0	931.0	552.4	600.0		
18	128.8	223.2	444.1	819.1	1010.8	759.7	1717.5		
19	128.4	222.8	444.3	821.1	1005.1	699.0	1373.9	600.0	
20	110.4	222.4	449.5	808.8	915.6	523.6	1463.7	1802.2	
21	110.6	222.4	449.6	809.2	915.0	513.5	1402.9	1620.1	400.0
22	97.7	213.9	441.2	793.5	857.5	399.3	1341.9	1932.6	953.0

b) h= 20.2 m

Strut \ Stage	1	2	3	4	5	6	7	8	9
1									
2									
3									
4	0.0								
5	200.0								
6	403.4								
7	291.3	200.0							
8	157.7	684.4							
9	217.1	241.7	600.0						
10	149.8	207.3	1078.5						
11	198.4	203.4	642.8	600.0					
12	183.2	149.3	604.9	1120.6					
13	190.4	177.8	595.1	734.4	600.0				
14	190.3	160.0	507.5	694.5	1499.9				
15	186.1	165.4	535.7	685.2	1130.6	600.0			
16	178.2	162.5	520.2	622.6	1128.7	1396.9			
17	175.1	160.9	525.4	640.9	1102.5	1065.8	600.0		
18	166.6	166.0	540.4	642.4	1057.8	1057.7	1558.0		
19	165.8	165.1	539.1	644.5	1066.9	1034.1	1178.1	600.0	
20	136.3	150.2	526.5	625.1	1009.5	925.7	1173.6	1709.4	
21	136.5	150.2	526.1	625.1	1010.9	924.0	1117.0	1514.1	40
22	135.9	158.4	537.8	626.7	988.2	858.2	992.1	1804.3	109

c) h= 17.7 m

[4] Since every strut is previously pre-loaded, the computed values reflect the apparent load on the strut

Strut \ Stage	1	2	3	4	5	6	7	8	9
1									
2									
3									
4									
5	200.0								
6	296.8								
7	184.4	200.0							
8	110.6	561.0							
9	171.5	114.4	600.0						
10	128.8	138.5	1064.4						
11	178.8	135.9	620.4	600.0					
12	158.3	94.6	638.4	1196.3					
13	166.2	125.1	631.1	794.5	600.0				
14	165.7	108.7	533.4	734.8	1579.6				
15	162.2	115.1	567.0	731.7	1172.7	600.0			
16	154.6	117.4	559.3	658.4	1092.9	1445.4			
17	152.4	115.6	566.5	686.2	1077.2	1090.0	600.0		
18	141.2	114.5	573.9	686.9	1025.4	1023.8	1657.7		
19	140.4	113.4	571.7	689.9	1047.7	1025.9	1279.9	600.0	
20	124.6	106.1	567.0	686.2	1049.2	936.8	1249.4	1675.8	
21	124.8	106.4	566.5	684.6	1049.9	944.1	1223.7	1451.4	400.0
22	118.0	103.3	565.5	682.0	1040.3	907.9	1154.2	1606.5	944.8

d) h= 12.6 m

Strut \ Stage	1	2	3	4	5	6	7	8	9
1									
2									
3									
4									
5	200.0								
6	395.8								
7	283.4	200.0							
8	149.0	699.4							
9	210.1	252.3	600.0						
10	104.6	189.4	1236.2						
11	154.8	187.2	790.7	600.0					
12	134.8	121.6	731.0	1193.8					
13	142.8	152.5	724.2	789.1	600.0				
14	134.8	135.3	595.5	658.3	1757.0				
15	131.6	141.8	630.2	656.8	1341.1	600.0			
16	121.3	142.7	613.0	546.0	1212.5	1311.5			
17	119.6	140.8	620.6	576.5	1200.1	927.9	600.0		
18	114.1	145.7	637.3	580.0	1127.8	840.7	1224.7		
19	113.9	144.3	634.9	584.2	1155.2	850.2	823.9	600.0	
20	103.0	140.5	639.4	590.5	1131.7	852.3	927.9	1764.7	
21	103.2	140.4	638.6	589.1	1133.9	863.3	926.0	1540.2	400.0
22	96.4	132.5	630.6	582.9	1122.7	842.9	855.0	1575.7	812.9

e) h= 10.1 m

Plotting the sum of the strut loads acting on struts 1 to 9 through the excavation depth in comparison with the computed struts loads assuming the struts are ideally elastic, it is clear that the external JGP solution is advantageous (Table 5.2). Although the reinforcement has practically no effect for excavations less than 16.1 m deep (6^{th} stage of excavation), there is a significant reduction in the strut loads (10-30 %) below the 7^{th} stage of excavation (depth 22.9 m) in the middle of the lower MC. Furthermore, at the last stage of excavation the sum of the loads carried by the struts is roughly the same for $h \geq 12.6$ m with a total average of 7100 kN/m. The development of these loads along the excavation process is very similar for h= 17.7 m and h= 12.6 m while for h= 20.2 m, at lower excavation depths the sum is much smaller; for instance, referring to h= 20.2 m , at the 7^{th} level of excavation, depth 22.9 m, the total load carried by strut 6 before the installation of strut 7 is around 880 kN/m compared to 1400 kN/m for $h \geq$ 17.7 m that means about 60 % more. Strut 6 is installed at RL 83.3 m and the LMC layer starts at RL 83.4 m; it is therefore evident here for h= 20.2, corresponding to the total coverage of the LMC, the effect of the ground improvement in reducing the driving force towards the wall and as a consequence in the pressure towards the struts.

The total sum of the struts load for the different cases presented is always less than the design capacity of the revised strut system (Table 4.2), selected for untreated case, with a total

maximum stress at the bottom of excavation of about 40 % the maximum capacity of the struts (≈7200 kNm/m compared to ≈18700 kNm/m).

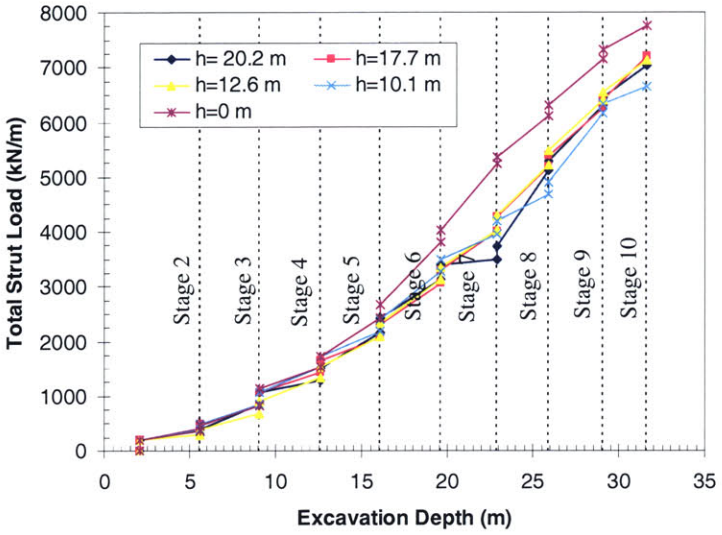

Figure 5.7-Sum of Struts Load as function of treatment thickness *h* through the excavation process

When *h*= 10.1 m the thickness of the treatment reaches RL 73.3 m (close to the final foundation elevation) and below the location of the last strut, a difference in the computed performance of the struts emerges; in fact the total load carried is about 15 % less than the other cases during the excavation process (Figure 5.7).

The maximum strut force generally occurs in the excavation step following its installation with the exception of strut 8 that for $h \geq 17.7$ m carries an higher load at the last stage of excavation. Very little change in load is computed in the 6th and 7th level struts after the 8th strut is installed and their individual load is almost constant until the bottom of excavation is reached with a force in the order of 1000 kN/m.

Comparing the computed maximum strut forces along the trench for the improved cases and the original one in elastic condition, it is evident that the maximum load carried by strut 5 in the original configuration at the 6th level of excavation (RL 83.3 m), is almost equal to the load carried by strut 8; there is practically no effect in the reduction of the load carried by struts 1 to 3

(Figure 5.8). Regarding strut 9, even if it is pre-stress to a lower value compared to the other strut (refer to table 4.2), it does not really contribute to the stability of the excavation; this especially because at that level most of the horizontal pressure coming from the soil and the wall is supported by the modeling JGP raft.

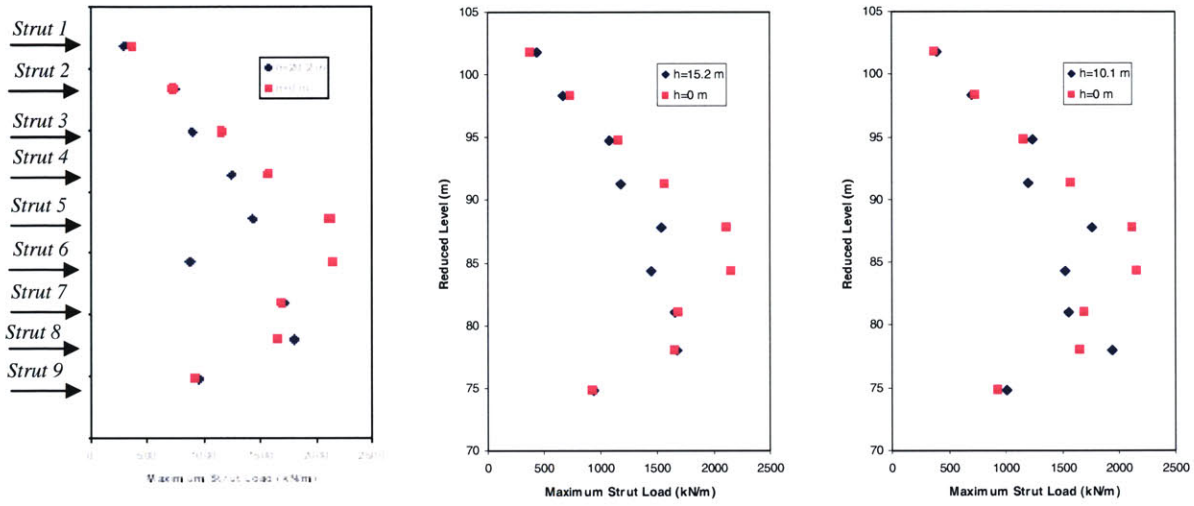

a) h= 20.2 m **b) h= 15.2 m** **c) h= 10.1 m**

Figure 5.8-Comparison of computed maximum strut forces for different thickness *h*

5.3 Effects of Treatment Strength Ratio *N*

This section describes the effects of the treatment strength ratio, $N = \frac{s_{uT}}{s_{u0}}$, on the excavation performance. The analyses assume full height treatment of the LMC (h=20.2 m) with full plan coverage. Δ=20 m and N=1⇒9.

5.3.1 Lateral Wall Deflections

From Figure 5.9 it is evident that different values of the ratio N do not influence significantly the computed wall deflection (N=1 corresponds to the situation without treatment). The wall deflected shapes look similar with N varying between 5 and 9; the maximum wall deflection is

obtained at the same level, 65.7 m RL, for the different cases, underneath the bottom of the excavation, with a value varying a little between 170 and 190 mm. Comparing Figure 5.4 and 5.10, it is evident that the variation of *N* has a higher effect in reducing the maximum wall deflection through the levels of excavation.

Practically this means that the design strength of the injected columns could be kept the same as the one used in the original design for the JGP slab installed between the edges of the trench (300 kPa).

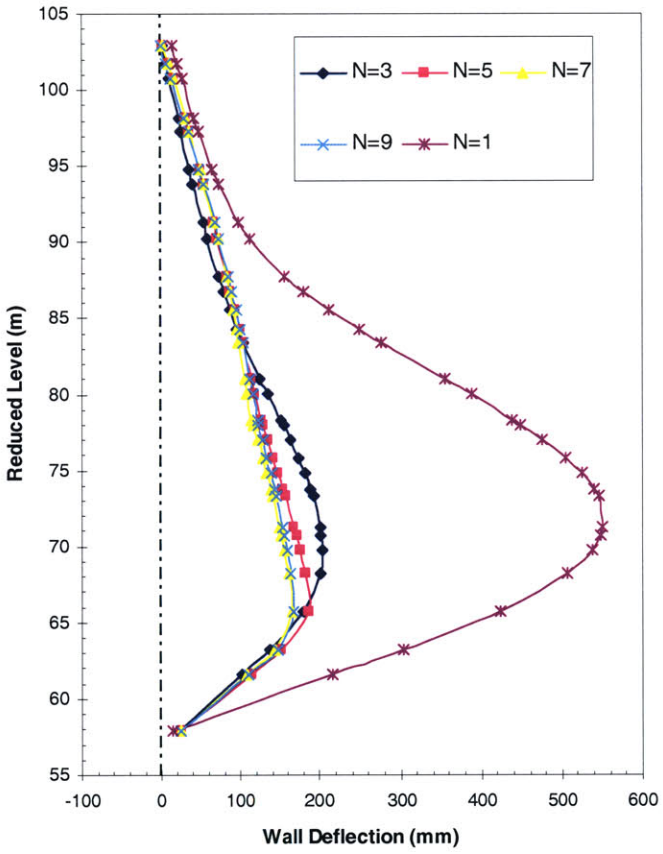

Figure 5.9-Effect of treatment strength ratio, *N*, on maximum computed wall deflection for excavation at RL. 71.3 m

Moreover, the results evidence that in order to propose the more efficient remedial solution for the problem, the geometry of the applied solution itself matters more than the design strength.

In fact experience demonstrates that in practice the measured strengths determined from unconfined compression test on core samples for grouted soils, are usually much higher than those declared in the specifications of the project as a result of the design process (Wong and Goh, 2006). Therefore there is no reason to make a series of conceptual decision from the interpretation of the computed data varying the *N* value if in reality the actual strengths obtained might probably be different and conservative. The controlling parameters relate to the geometry of the treatment zone more than the strength parameters.

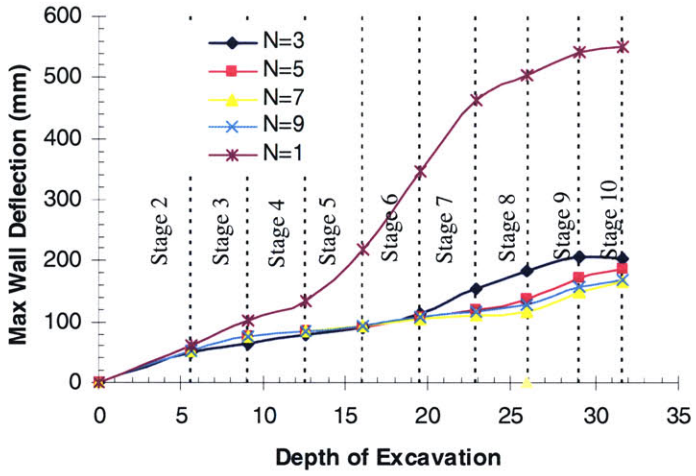

Figure 5.10-Maximum computed horizontal deflection against excavation depth for different values of treatment strength ratio *N*

5.3.2 Wall Bending Moments

Figure 5.11 shows plot of the bending moment curves while excavation proceeds, as function of the variable *N* ; for the all cases presented the maximum moment is reached at level RL 64.5 m on the positive side. The results in figure 5.11 show that the ratio *N* has practically no effect in the variation of the bending moment acting on the wall.

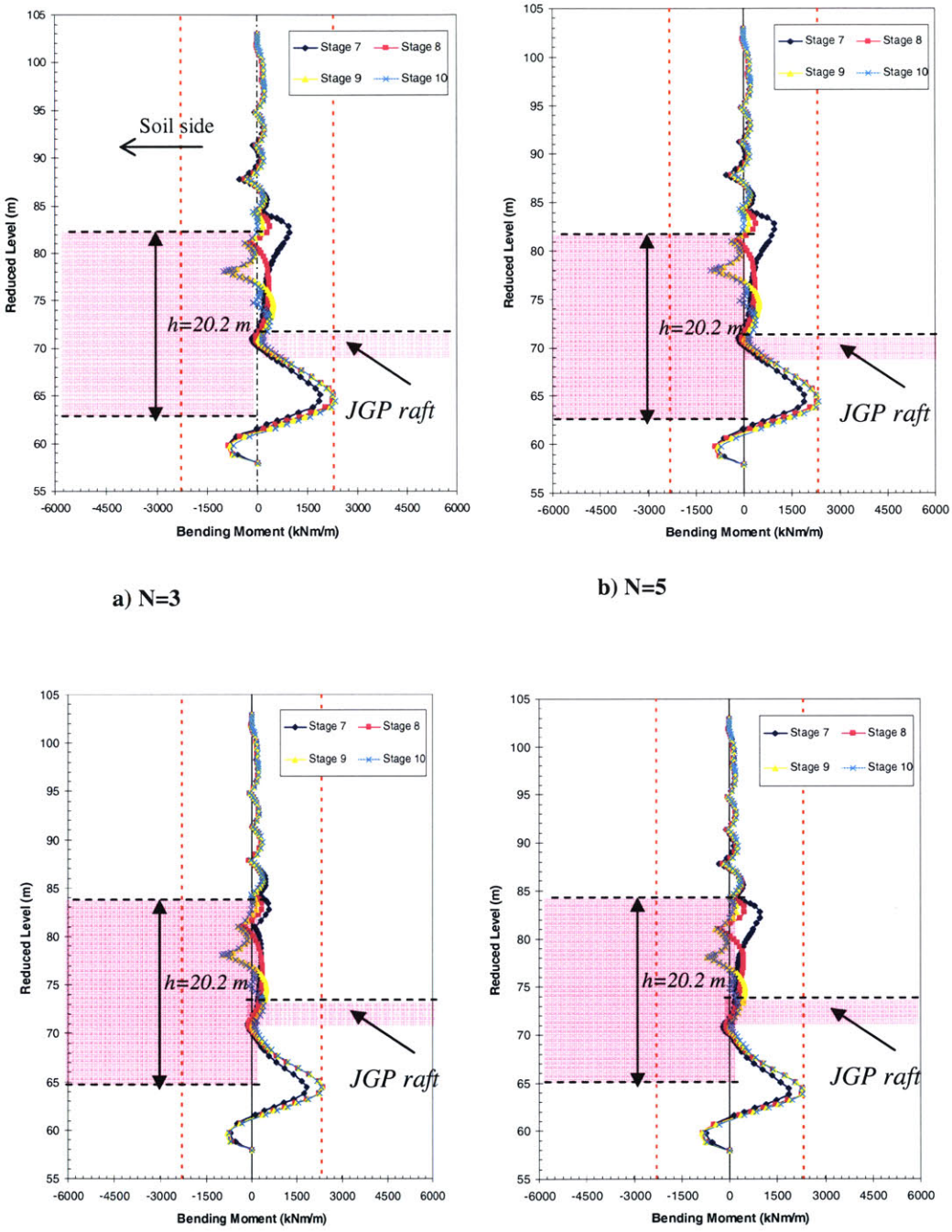

a) N=3

b) N=5

c) N=7

d) N=9

Figure 5.11-Computed bending moment acting on the diaphragm wall as function of treatment strength ratio *N* for stages 7 to 9

5.3.3 Strut Loads

Results for the strut loads obtained varying the N ratio are plotted in figure 5.12. It is here evident that increasing the N value determines a lowering in the sum of the load carried by the struts where in fact the driving force toward the wall is also lowered.

Along the excavation process, strut 8 is the one experiencing the highest load; the effect of the improvement on the maximum computed values of forces acting on the struts is evident starting from the 4th strut with an average reduction in the load of about 70 % compared to the original design (figure 5.13).

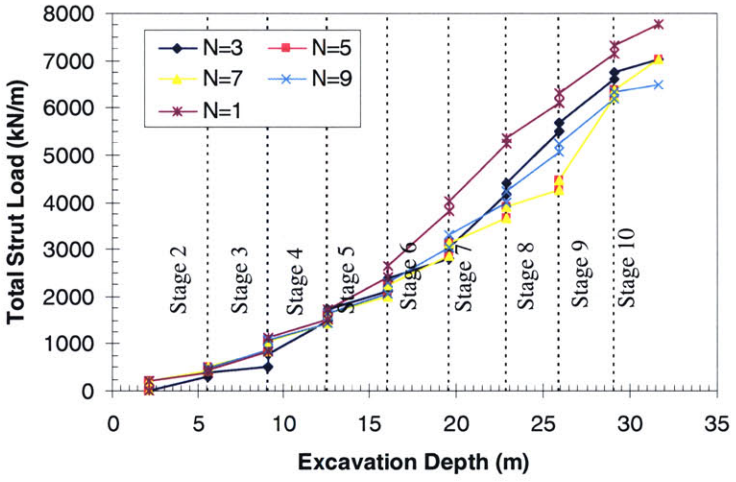

Figure 5.12-Sum of Struts Load as function of treatment strength ratio N through the excavation process

Except for extreme values of the variables considered, the performance of the deep excavation in terms of the strut load is not really significant and this confirm what said before regarding the choice of the N ratio as the decisive parameter to consider in the evaluation of the problem.

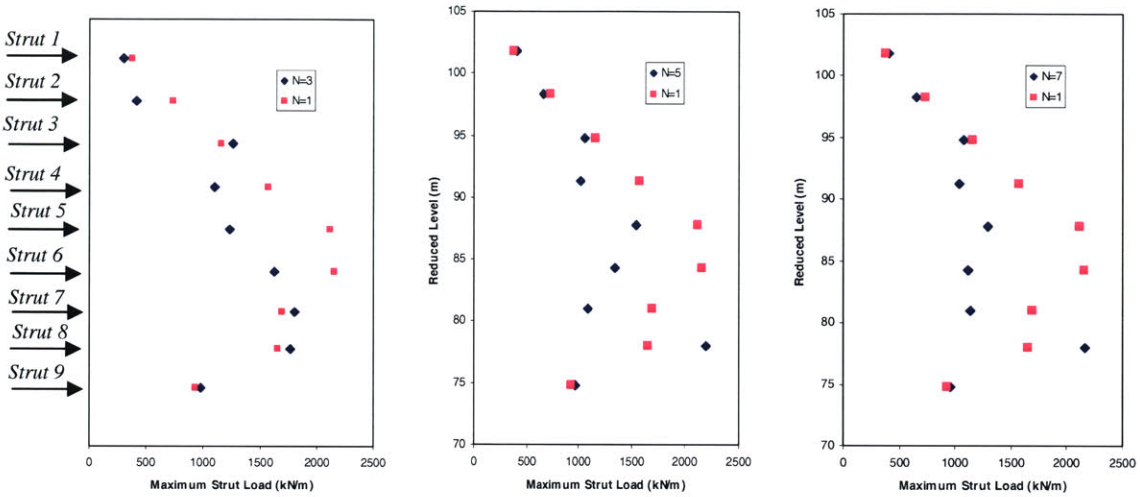

a) N=-3 **b)N=5** **c)N=7**

Figure 5.13-Comparison of computed maximum strut forces for different values N of the strength ratio of the treatment

As a matter of fact, the curves presented in figure 5.13 confirm the beneficial effect of the solution proposed in terms of the overall stability of the excavation but at the same time evidenced that the recommendations presented later on do not have to refer to the effects on the strut as decisive factor in order to propose the best solution.

5.4 Effects of Percentile Plan Coverage of Treatment

5.4.1 Lateral Wall Deflection

As mentioned before, the distribution and geometry of the grouted columns is also determined by its coverage in plan. It is obvious that the cost of the remediation scheme will vary significantly according to the percentage of plan coverage. Results from a parametric study on the impact of the coverage of the improvement are here highlighted.

Figure 5.14 shows results for the maximum wall deflection at the last stage of excavation (RL 71.3 m) considering a coverage in plan of 30 %, 50 %, 80 % and 100 % and comparing it to the case with no treatment. For these results values of Δ=10 m, N=7.5 m (s_u= 300 kPa) and a thickness of treatment h= 20.2 m have been considered.

It is immediately evident that a coverage of 30 % is not really advantageous if compared to the original situation (0 %); in fact even if the bottom of excavation is reached, the maximum wall deflection is much more than the one computed for a coverage $\geq$ 50 % (figure 5.14). It is also evident that for a plan coverage $\geq$ 50 %, the deflected shape of the wall for the last stage of excavation is almost identical. This result has an important impact in terms of costs and time for the project; comparison and evaluation of other results (struts loads, bending moment etc.) is nevertheless fundamental.

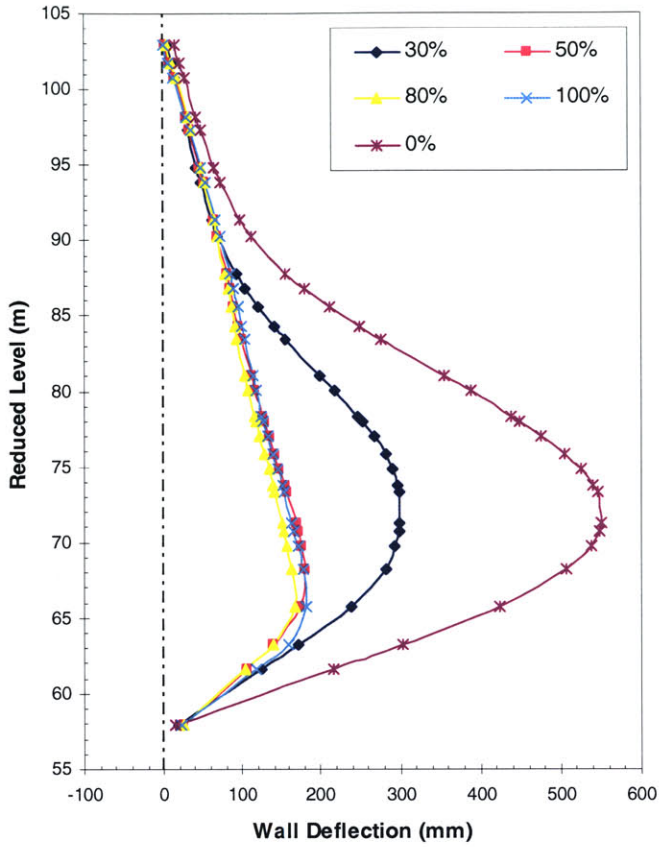

Figure 5.14-Effect of plan coverage in percentile points, on maximum computed wall deflection for excavation at RL. 71.3 m

5.4.2 Wall Bending Moments

Despite of the results for the lateral wall displacement (Figure 5.14), the variation in the percentage of plan coverage of the improvement has a profound impact in the development of the bending moment (Figure 5.15). The wall, with a coverage of 30%, experiences high moments on both sides even at shallow depths in correspondence of the struts and there is likely the formation of multiple plastic hinges increasing the possibility for a collapse to occur. Rising the plan coverage gradually determines the lowering of the negative moment on the retained side of

the wall and, as already seen in evaluating other parameters, the potential formation of a plastic hinge at level RL 64.5 m close to the toe of the wall.

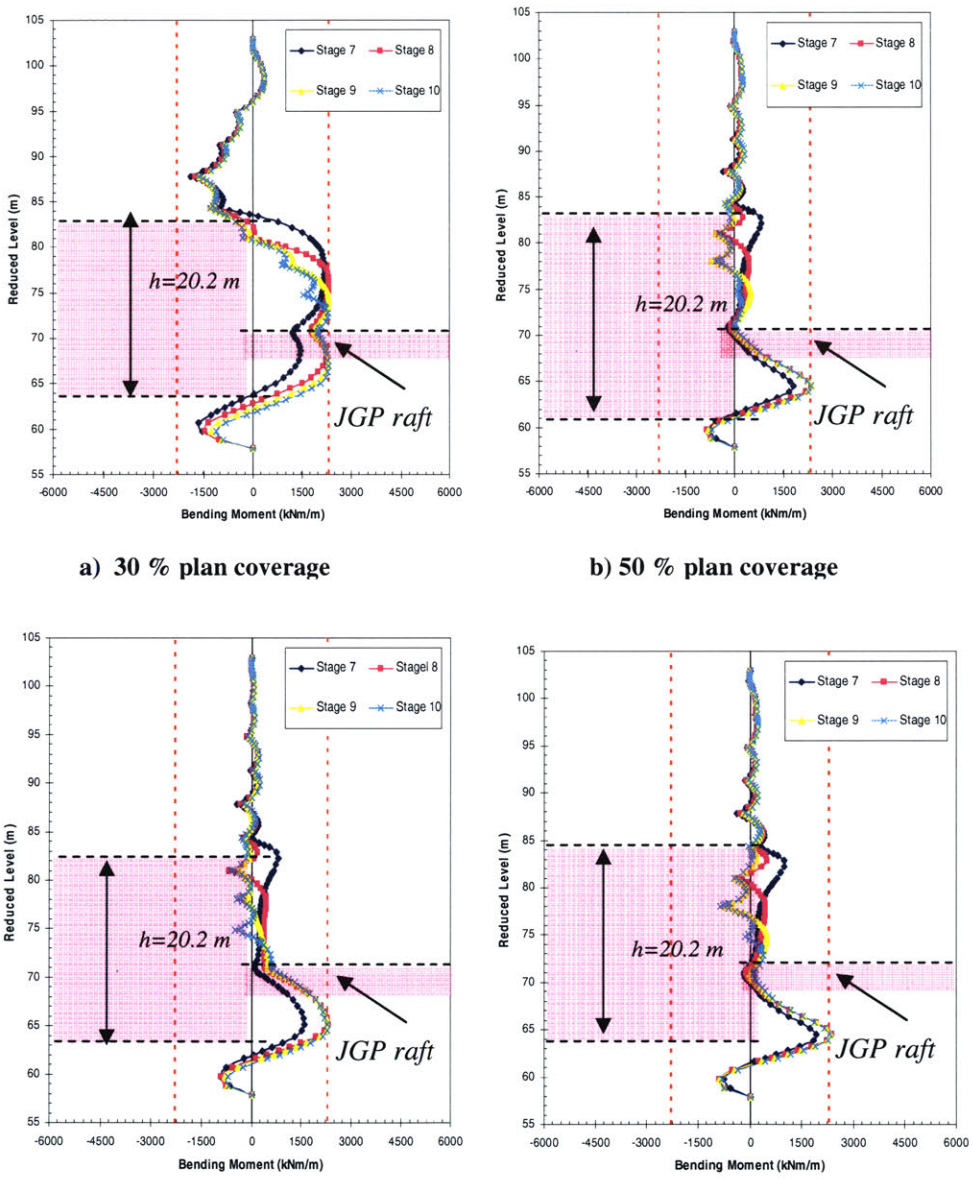

a) 30 % plan coverage

b) 50 % plan coverage

c) 80 % plan coverage

d) 100 % plan coverage

Figure 5.15-Computed bending moment acting on the diaphragm wall as function of percentile plan coverage for stages 7 to 9

5.4.3 Strut Loads

Even though the results for the wall displacement and the bending moment as a function of the plan coverage demonstrate an advantage in the application of this solution; focusing on the loads carried by the struts during the excavation process, it is evident that a coverage of 30 % does not have a notable effect while for a percentage ≥ 50 % there is a overall reduction of about 12 %. A total plan coverage of the area behind the wall with the treatment is therefore not entirely justified in a practical application since it implies a significant increase in the cost of the project when similar prediction can be obtain with a coverage of 50 % or 80 %.

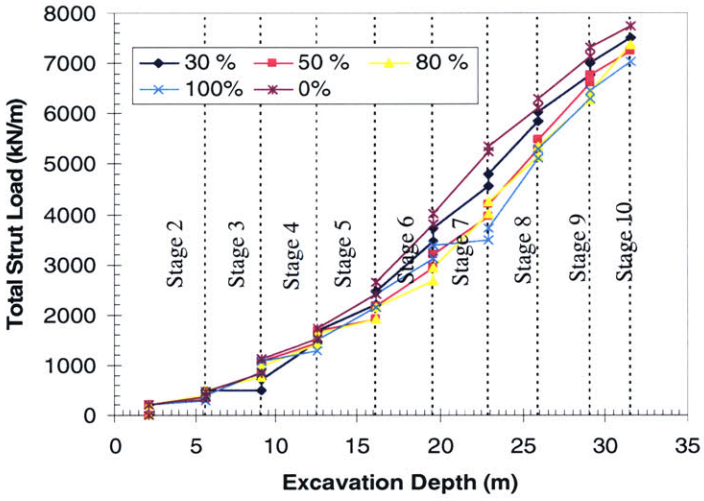

Figure 5.16- Sum of Struts Load as function of % plan coverage through the excavation process

Comparing the results in figure 5.17 it emerges that , keeping the same typology of struts in the parametric evaluation, the effect of the solution is evident with a coverage ≥ 50 %. Strut 8 at RL 77 m is stressed at about 35 % less than the solicitation on the elastic case. In particular, strut 8, the one experiencing the high loads through the excavation, it experiences an axial load of about 55 % .

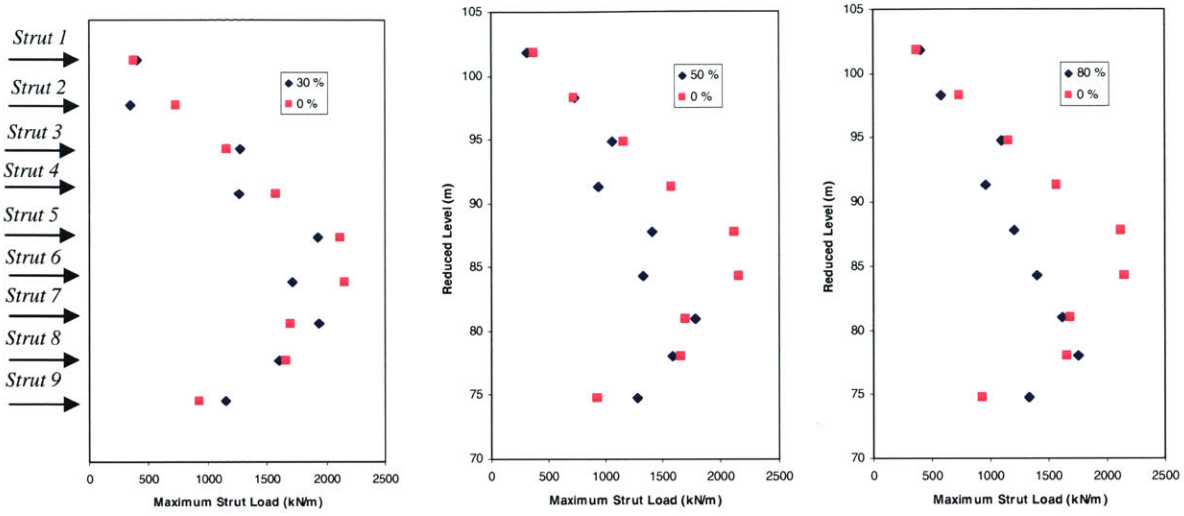

a) 30 % plan coverage **b) 50 % plan coverage** **c) 80 % plan coverage**

Figure 5.17-Comparison of computed maximum strut forces for different values in% of the plan coverage of the treatment behind the excavation

5.5 Effects of Horizontal Extension of Treatment Δ behind the Wall

5.5.1 Lateral Wall Deflections

Figures 5.18 a,b,c summarize the wall deflected profiles for three different cases, all characterized by the same undrained shear strength value for the soil cement mix and a different horizontal extension of the treatment behind the wall, and a fixed h=20.2 m, 17.7 m and 12.6 m, respectively.

In fact, as first sight it appears that for the same value of h, the lateral extension of the treatment behind the wall reduces the maximum computed wall deflection. In fact , except for h= 12.6 m , increasing laterally the treatment in steps of five by five meters causes a reduction of the maximum wall deflection of 50 mm every step. In reality, even if the positive effect of the treatment is evident, it is necessary to take into account the costs related with an increased lateral extension of 5 meters and if these expenses are really worth in order to achieve 50 mm of control in the wall movement.

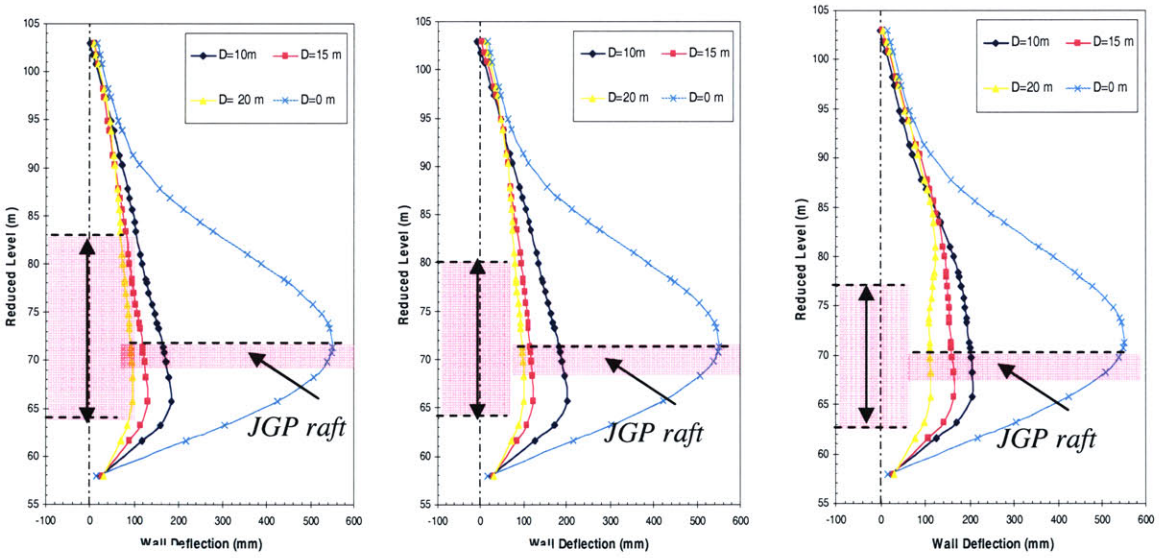

a) h= 20.2 m **b) h= 17.7 m** **c) h= 12.6 m**

Figure 5.18-Effect of lateral horizontal extension of treatment, on maximum computed wall deflection for excavation at RL. 71.3 m

5.5.2 Wall Bending Moments

Practically no effect results from the lateral extension of the improvement Δ (N=7.5 considered) on the bending moment acting on the wall (Figure 5.19) for the levels of excavation that manifest the higher risk. As soon as the excavation proceeds, the bending moment is contained to small values compared to the yielding capacity of the wall and it reaches a maximum value of 2360 kNm/m, exceeding the bending capacity of the wall only at RL 64.5 m, in the LMC underneath the final foundation elevation. Temporarily, through the consecutive stages the bending moment has approximately the same values along the profile of the wall.

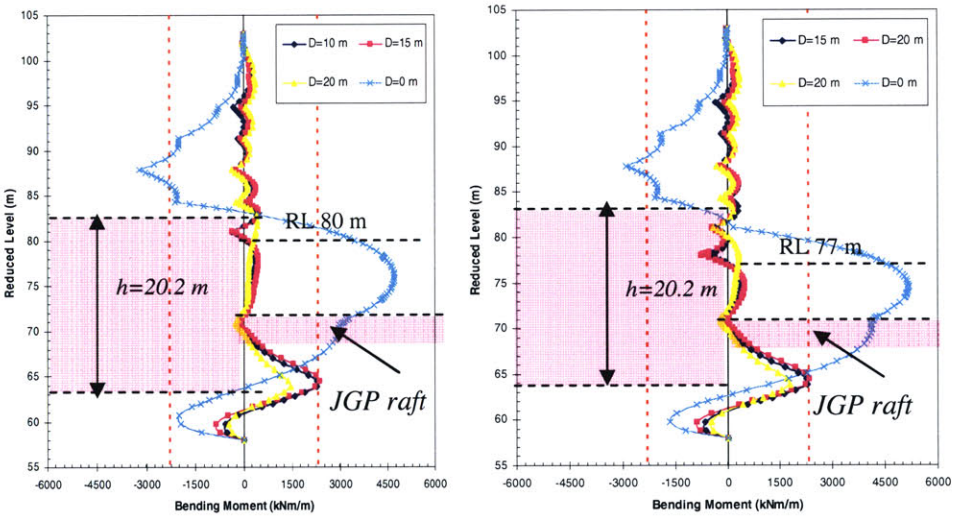

a) Excavation at RL 80 m **b) Excavation at RL 77 m**

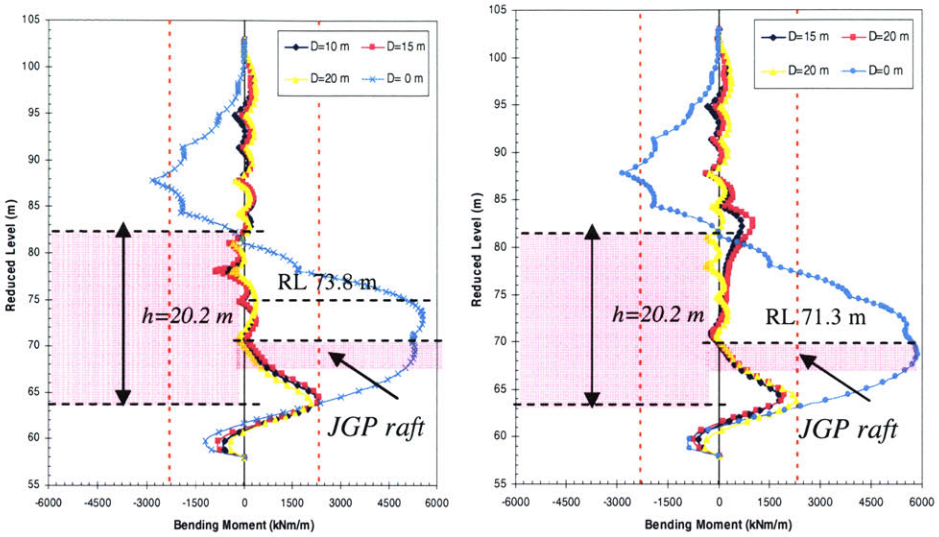

c) Excavation at RL 73.8 m

d) Excavation at RL 71.3 m

Figure 5.19-Computed bending moment acting on the diaphragm wall as function of lateral extension of treatment Δ for excavation from RL 80 m to RL 71. 3 m

5.5.3 Strut Loads

Figures 5.20 and 5.21 summarize prediction for the axial loads acting on the struts considering as primary variable the lateral extension Δ of the treatment behind the wall. For Δ= 10 m and Δ= 15 m there is a reduction in the total sum of the strut loads of 11 % in comparison to the case with no treatment; the treatment seems to be positively efficient in particular starting from the excavation depth of 19.6 m, corresponding to the 6^{th} level of excavation. If a Δ value of 20 m is considered, there is a further decrease in the loads at depth 25. 9 m , 8^{th} level of excavation, reaching at the bottom of excavation a reduction of the loads of 20 % compared to the original case.

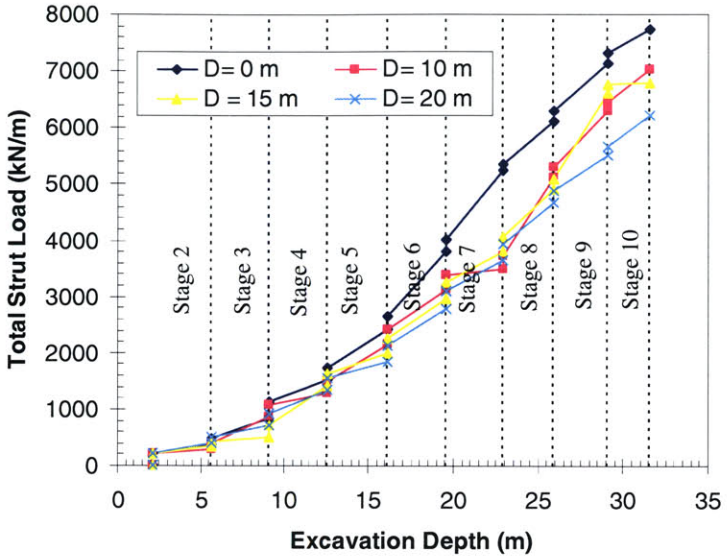

Figure 5.20- Sum of Struts Load as fucntio of the horizontal extension of the treatment Δ behind the wall through the excavation process

All the struts work maximum at 60 % of their load capacity and they work efficiently especially in correspondence of RL 84. 3 m (strut 6) where there is a reduction of the load for the single strut of roughly 50 % .

Regarding strut 9, as already shown for other variable, the maximum load equalize the one for the original case with the exception of Δ= 20 m where strut 9 mobilized a load that is 25 % less.

Not significant results are computed for the first levels of struts, until RL 94. 8m.

Again, the efficiency of the solution proposed in contain and control the structural actions on the characteristic elements of the excavation in correspondence of the location of the lower marine clay is here clearly demonstrated.

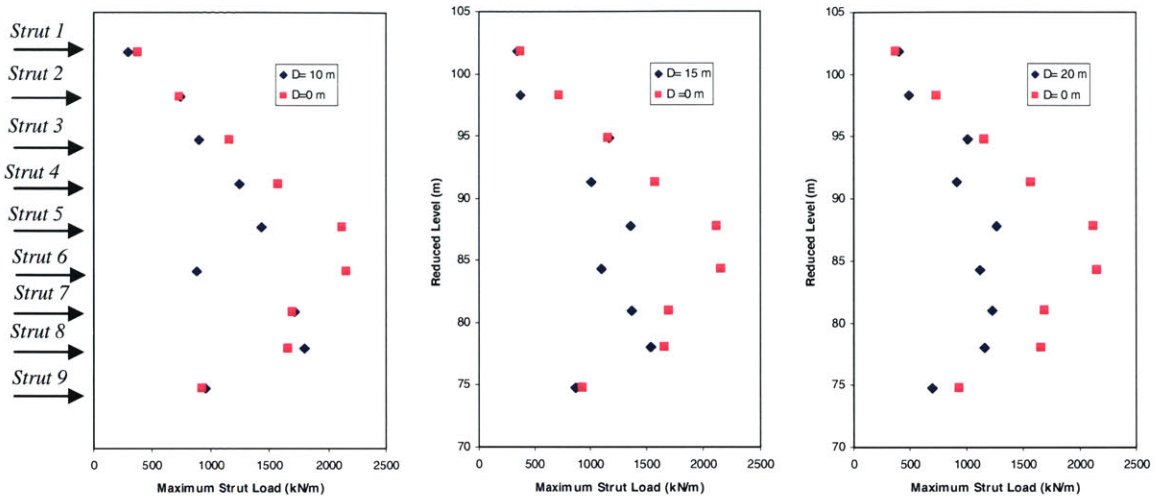

a) Δ= 10 m b) Δ= 15 m c) Δ= 20 m

Figure 5.21-Comparison of computed maximum strut forces for different values Δ of the plan coverage of the treatment behind the excavation

5.6 Axial Load and Strain on existent JGP

Section type K, considered in this study, has a single layer of jet grouted piles (JGP), formed between the side walls before the beginning of excavation which was designed with a thickness of 1.5 m (starting at the bottom of excavation at RL 71.3 m until RL 69.8 m). As mentioned before, the main aim of this slab is to act as a strut and support part of the axial load coming from the wall displaced by the excavation progression.

For the entire system to be effective the resistance of each element must be greater than the loads imposed on it. Figure 5.22 evidences the typical loads encountered in a JGP slab. Jet grout piles are therefore designed to resist mainly to wall deflection and to limit the bending moment acting on the wall itself.

As the slab is stressed while proceeding with the excavation different modes of failure are potentially possible (Page et al., 2006):

-Buckling

-Bending

-Continuity of load path

-Stress/strain behavior of improved soil

To integrate and complete the analysis presented until this point it is therefore interesting to evaluate the effect of the external soil treatment on the axial load acting on the JGP and also the effect on the strain determined by this load too.

Figure 5.22 shows the development of forces along the JGP slab for the different stages of excavation obtained from two different analysis: one that refers to the original intact situation of the site, with no treatment (h=0 m) and another one modeling the LMC as entirely treated in its vertical extension (h=20.2 m) with an horizontal extension of the treatment Δ= 10 m and a s_u value for undrained shear strength of the treatment of 300 kPa. The forces are also compared to the theoretical design capacity of the JGP defined as a band taking into account the case with and without friction and determined from the following relationships: $F_h = B(\sigma_v+2s_u)$ and $F_h = B(\sigma_v+2.3s_u)$ with B=1.5 m thickness of the JGP slab and s_u undrained shear strength along the profile.

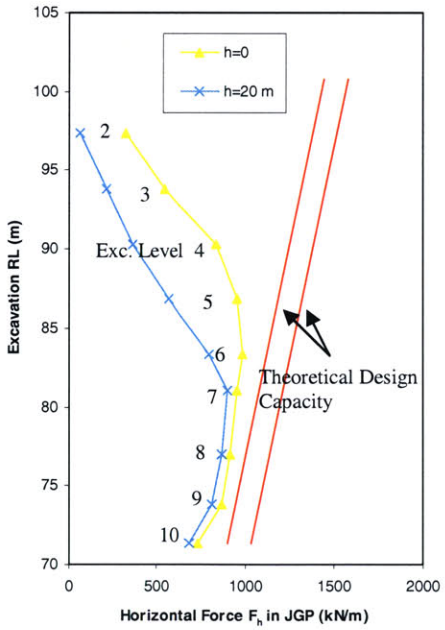

Figure 5.22- Effect of analysis method on computed horizontal force in JGP

It is immediately evident that even though the computed horizontal force for the case with no treatment does not completely mobilize the resistance of the slab itself, the effect of the improvement can reduce it of a significant amount, especially at more shallow depth.. This effect is slightly less evident for the last 4 stages of excavation.

Mobilization of the passive resistance in the JGP layer is correlated with the axial compression that the slab experiences. Figure 5.23 presents the corresponding axial compression of the JGP layer computed for the two cases previously mentioned through the excavation stages.
The effect of the soil improvement is evident starting from the 4th level of excavation (RL 90.3 m) and increasing with excavation depth. After the 7th level of excavation the deviation between the two computed cases is nearly constant at about 70 % in reduction.

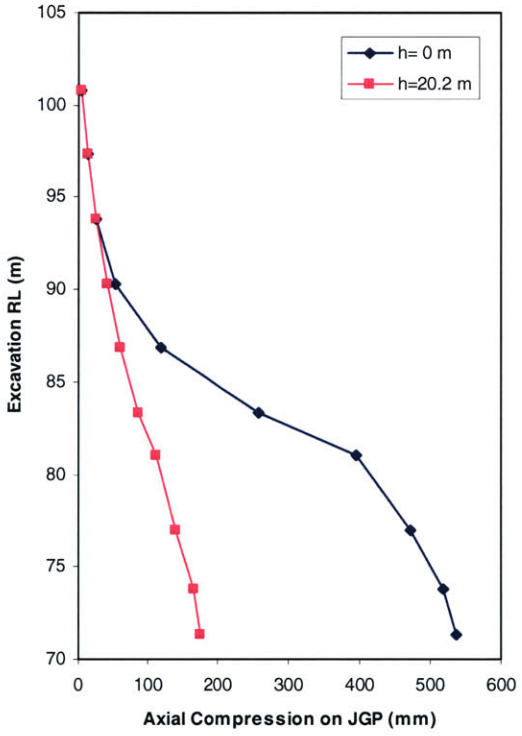

Figure 5.23- Effect of analysis method on axial compression in JGP

In particular, when considering the Mohr-Coulomb model, once the material reaches failure it is assumed that it can sustain the yielding load until a maximum strain is reached. In reality, and this holds in particular for cemented and soil-cement mix materials, the typical stress-strain behavior may shown strain softening after reaching failure, as shown in Figure 5.24.

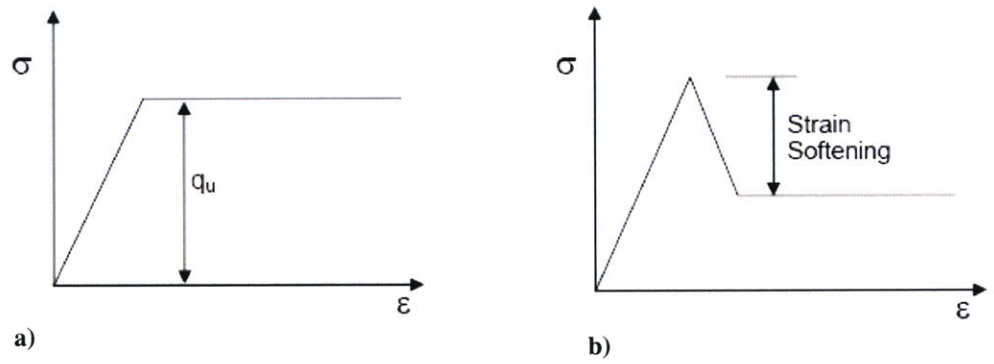

Figure 5.24- Modeling of stress-strain behavior of JGP (a) elastic perfectly-plastic; and (b) strain softening
(Wong, and Goh, 2006)

From samples tested conducted under different confining pressures, the JGP material exhibits either brittle or strain softening behavior. The strain at failure increases with increasing confining pressure but in general it ranges between 1.2 % and 4% (Wong, and Goh, 2006); going back to Figure 5.24, in the case with no treatment (h=0 m) the maximum computed strain is of 3.5 % obtained from the computed horizontal displacement applying the following relationship:

$$\varepsilon_a\,(\%)=\Delta L/L*100=2*\,\Delta u_h/30m*100$$

and dangerously close to the maximum strain accepted by the material. Even tough in this study the effect of strain softening has not been modeled, it is important to notice that the reduction effect obtain with the treatment permits to contain the maximum strain at 1.1 % and it keeps the strain curves on the first portion of the curve, before softening happens and where the resistance of the system increase with strain.

6. EXTERNAL JET GROUT AS RETROFIT SOLUTION

6.1 Introduction

The analyses in Chapter 5 have identified the main parameters for the proposed external ground treatment solution in controlling the performance of an excavation support system. The results identified clearly the dimensions of the treatment zone needed to control wall deflections, bending moments and strut loads for a typical section (Type K) of the deep excavations for Circle Line Contract C824. This chapter considers the performance of the proposed treatment scheme to remediate the partially excavated section Type K.

The previous chapter has modeled the performance of the excavation support system enhanced with external ground treatment. This chapter follows the history of the excavation at section K. At the time of the Nicoll Highway Collapse (section M3, M2), the excavation at Type K had reached a depth of about 20 m (6^{th} level of excavation) and the diaphragm walls had deflected inwards by up to 400 mm. The excavation was subsequently infilled.

This chapter considers external ground improvement as a retrofit solution to enable completion of the excavation at section K. The computational model considers the entire process of excavation, backfilling, external ground treatment and re-excavation. Full details of the FE model are presented in Appendix B.

Based on the results presented in Chapter 5, this chapter considers a more limited series of parameters for the external ground treatment (Table 6.1).

Table 6.1- Values of variables analyzed for this study

h (m)	N	% coverage	Δ (m)
18,20	7.5	50,100	10

The following sections describe the results for this retrofit application focusing on ground treatment parameters needed to control performance during this re-excavation phase.

6.2 Excavation Sequence

The original design included ten stages of excavation from RL 102.9 m to RL 71.3 m (for a total depth of 32 m). After every stage of excavation is completed, steel struts are installed from wall to wall and appropriately pre-stressed (pre-load levels correspond to 50 % of the maximum expected strut load). In section Type K, the 6th level of excavation (RL 83.3 m), was reached on 20 April 2004 and at that point inclinometers installed along the walls recorded a maximum wall deflection of about 422 mm.

The new model here described, goes through the different excavation stages until the 6th, with input of the original design values used for the struts (Whittle, 2005) and, applying a specific feature of *PLAXIS,* a maximum wall deflection of 400 mm is obtained at the end of excavation 6[1]. Successively, the trench is completely backfilled with a drained fill material and struts left in place. The external ground treatment is now installed and model as in Table 6.1 while the struts during the re-excavation are changed with new pre-stressed ones in order to increase the effectiveness of the ground treatment in controlling the wall deflection and bending moment (Table 4.2)

6.3 Computed Results

6.3.1 Initial Partial Excavation

Figure 6.1 shows the development of the horizontal displacement of the diaphragm wall for the initial 6 excavation stages. It is immediately evident the significant increase in deflection from the 4th stage of excavation, having δ_{max}= 131 mm to the 5th stage where the maximum deflection reaches a value of 230 mm at RL 86.8 (Upper Marine Clay); these computed results agree quite well with the data measured from the inclinometer on the wall. The stage if excavation 6 has been appropriately modeled to have a δ_{max} of about 400 mm (the model gives δ_{max}= 402 mm at RL 78.35 m, in LMC)[2]. While proceeding with the excavation the elevation level, at which the

[1] Note: δ_h max of 400 mm is effectively assigned as input data for the model.
[2] This stage of excavation is only partially completed (with ΣMstage= 0.62 in *PLAXIS*)

maximum deflection is reached, moves downward along the wall length and as soon as it reaches the Lower Marine Clay, there is a sudden increase in the movement.

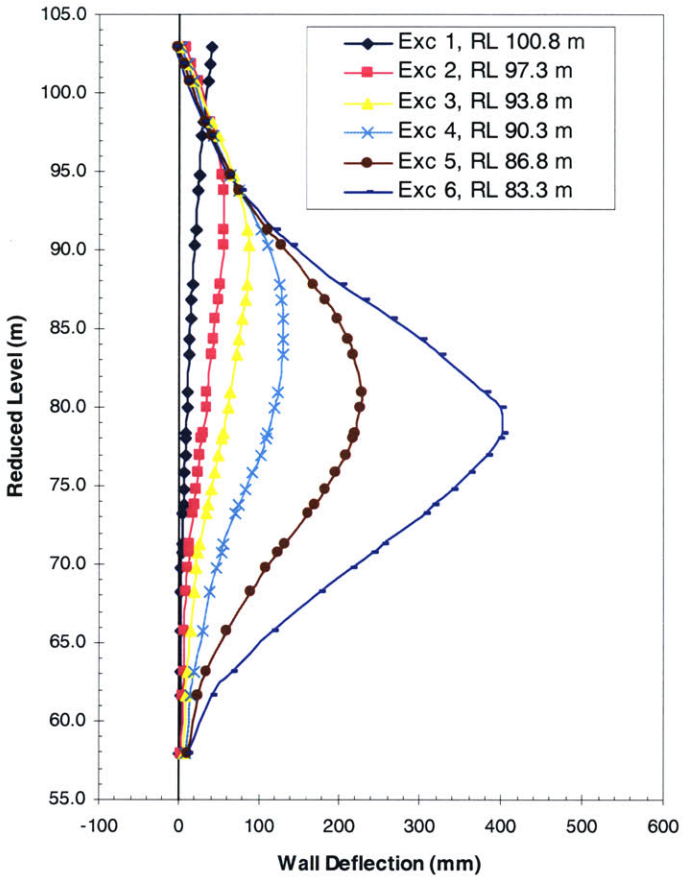

Figure 6.1 -Wall deflected shapes for original design

The bending moment acting on the wall during this stages is represented in figure 6.2. Looking at this plot it is evident at first sight that the moment increase considerably with the 5th stage of excavation (RL 86. 8 m) and the yielding capacity of the wall, represented by the hyphened line, it is reached on the right side of the wall, facing the trench, it is seriously approached with a M_{max}= 2290 kNm/m at RL 79 m, in the LMC. The situation turns more critical proceeding with the excavation; in fact when the level of the cut is at RL 83.3 m, right above the layer of LMC,

the bending moment slightly reaches its maximum value to stay in the elastic range in correspondence of three locations along the wall. Completion of the stage 6 of excavation would hence bring the wall to collapse due to the formation of a mechanism with rotation of the toe and two plastic hinges. This behavior is not fully representative of section K as the soil profile assumed is based on worst case conditions and soil properties (for the study of the collapse at M3).

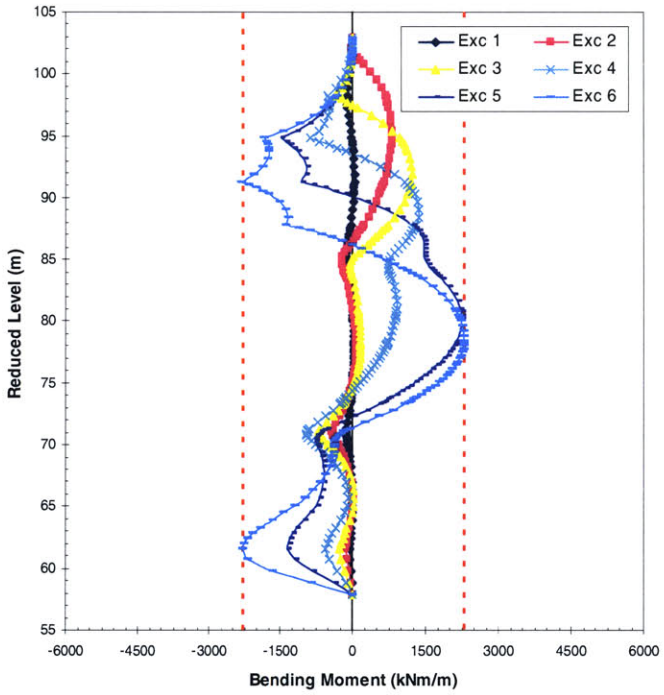

Figure 6.2 -Wall bending moment for original design

6.3.2 Backfilling

Once excavated until the 6th level, the entire trench was backfilled. Figure 7.4 shows the computed values for wall displacement and bending moment during this process.

The maximum horizontal deflection of the wall decreases by a small amount before the trench is completely backfilled, from 402 mm to 311 mm. Comparing the shape of the wall from figure

6.3 and 6.4 it is clear that infilling does help to reduce wall curvature and bending at RL 61.6 m, corresponding to the division between LMC and Old Alluvium layer.
Even though the wall is dangerously deflecting, the passive resistance due to the fill contribute to decrease the bending moment of the wall and take away the risk of a potential failure.

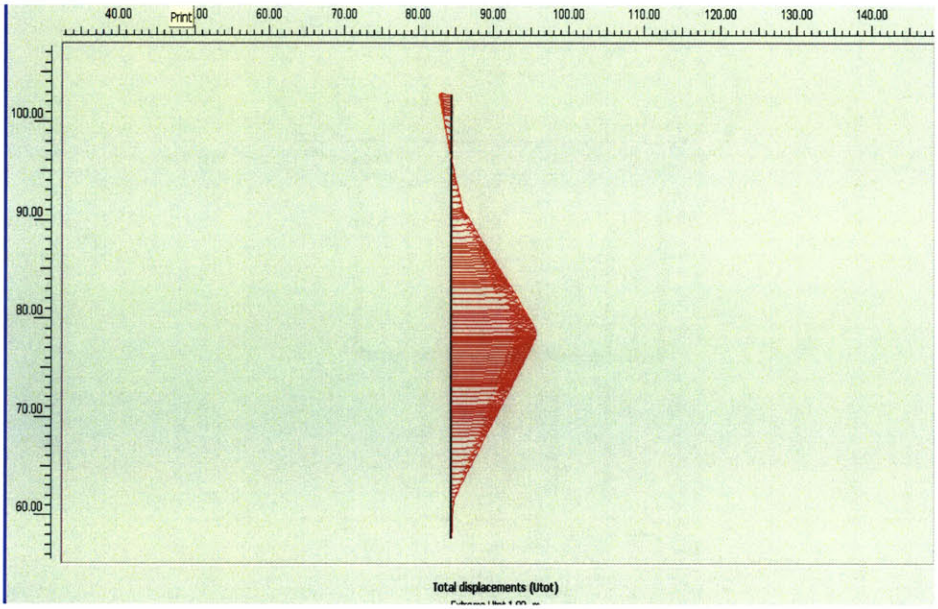

Figure 6.3 – Collapse mechanism for complete of 6th excavation stage (ΣMstage=1.0)

6.3.3 Re-Excavation

Once the entire excavation has been back filled, the proposed ground treatment is installed and the excavation restarted. Here will be plotted results for the case with a vertical thickness of treatment h=20.2 m, a lateral extension Δ=10 m behind the wall, a percentile plan coverage of 50 % and an undrained shear strength for the soilcrete mix of 300 kPa (N=7.5), combination considered to be the most effective among the different ones from Table 6.1. Figure 6.5 shows the computed wall deflections during re-excavation with a new set of pre-loaded struts (see Appendix B for details).

The results show very small incremental wall deflections above RL 88 . However, re-excavation produces an incremental maximum wall deflection of 100 mm below RL 80 m.

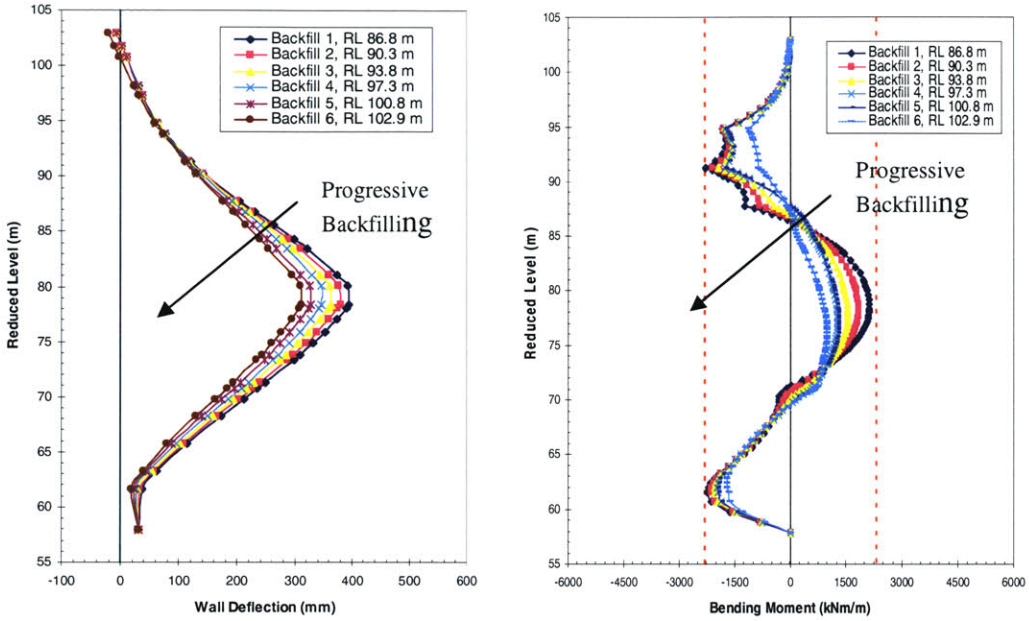

Figure 6.4 - Wall deflected shapes and bending moment for backfilling process

Despite of the fact that the wall exhibits a maximum horizontal displacement of about 400 mm, the structural behavior of the wall is much improved by reducing the bending moment. Figure 6.6 shows in fact that the moment capacity of the wall is only exceeded at RL 64.5 m, in the LMC. This single hinge prevents further load transfer downwards into the Old Alluvium, but is not sufficient to produce a mechanism or limit the stability of the excavation.

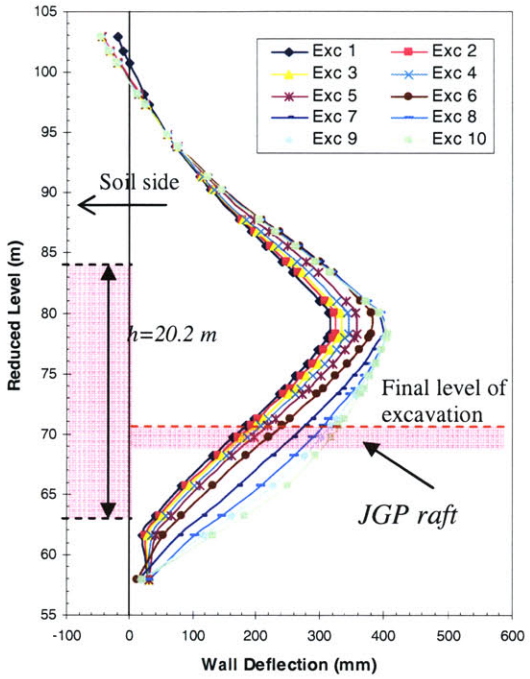

Figure 6.5 - Wall deflected shapes during excavation after treatment

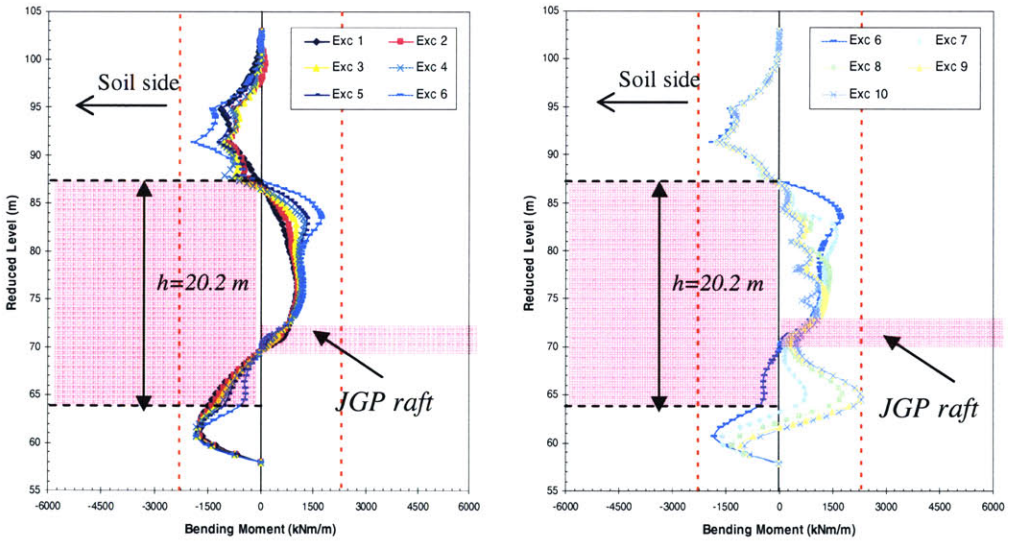

Figure 6.6 – Wall bending moment during excavation after treatment

Figure 6.7 compares maximum strut loads for the initial excavation and re-excavation stages. It is not possible to make a complete comparison on the development of the struts while proceeding with the excavation since initially the trench has been excavated only until level 6th. It is nevertheless obvious that the struts levels 1-3 are loaded much less after the improvement. In the re-excavation larger struts can be used hence high compressive loads in levels 4-10 can be correctly re-designed (with increased strut capacity and re-designed strut-waler connections). This model takes into account only one trial set of struts to achieve a better control of the process of excavation but it is true that the old strut can be easily replaced with other having high axial ultimate strength. The main aspect here to bring to the attention is that the ground treatment does not overload the struts.

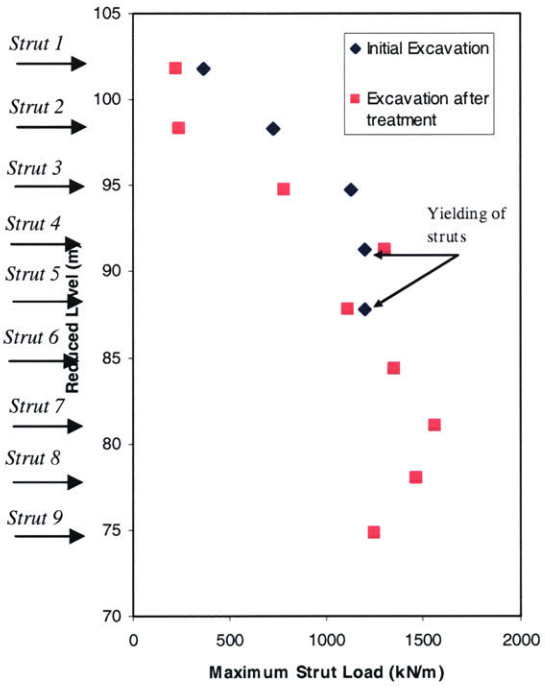

Figure 6.7 – Computed maximum strut forces during excavation before and after treatment

The last aspect that needs to be considered in the analysis is the effect of the proposed external treatment on adjacent ground and structures during re-excavation. In fact the subway alignment is located in a very sensitive area, with important commercial buildings very close to the site. The closest building is located about 20 meters from the excavation. Most of these buildings in Singapore are built on piles therefore extremely sensitive to the lateral movement of the soil induced for instance in this case by the excavation.

From the parametric study here conducted, a series of cross section has been traced to evaluate the lateral displacement of the soil at various distance behind the wall (figure 6.8).
The total lateral movement as might be logical to predict, decrease with the distance from the wall and its maximum value, for a distance of about 20 m is 300 mm. Comparing Figure 6.8 a) and b) it is evident that, for a distance of 20 m from the wall, the maximum incremental movement is about 130 mm, so almost 50 % of the total incremental movement registered after the entire process of excavation and re-excavation.

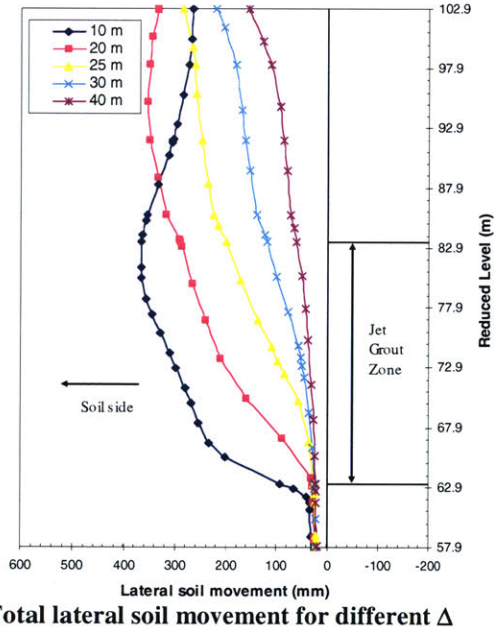

a) Total lateral soil movement for different Δ

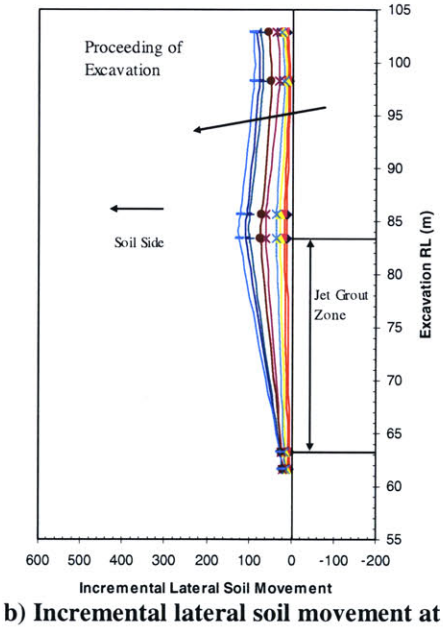

b) Incremental lateral soil movement at Δ=20 m

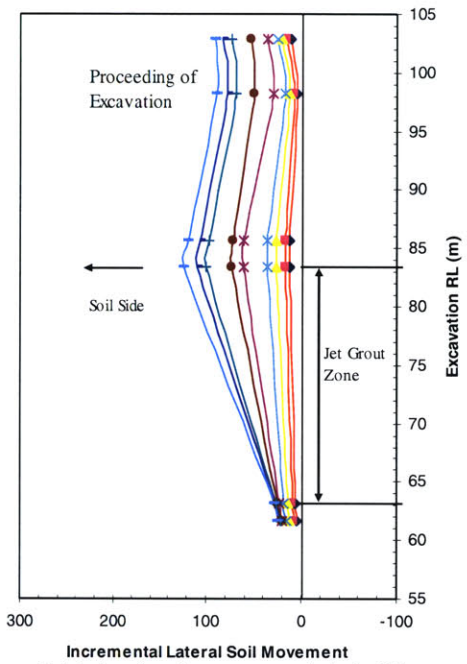

c) Incremental lateral soil movement at Δ=20 m, zoom in

Figure 6.8 – Lateral soil movement after treatment

Therefore, the treatment installed, while it can limit the overall amount of additional wall deflection induced in the wall during the all process of excavation, it does not isolate the effect of the excavation between the wall and the soil behind it. A more detailed analysis needs here to be carried out to evaluate the effect that the movement can have on the lateral displacement of piles on the foundations of the buildings.

7. SUMMARY, CONCLUSIONS AND RECCOMENDATIONS

7.1 Summary

The main aim of this thesis was to investigate the effectiveness of an external ground remediation technique in improving the performance of a deep braced excavation through parametric numerical analysis. The task was primarily motivated by the recent collapse of the Nicoll Highway during construction of the new Circle Line in Singapore (MFISH,2006). This project involved excavations greater than 30 m deep within soft marine clays. The proposed ground improvement system uses jet grouting, or deep soil mixing, to strengthen the Lower Marine Clay within the retained soil. The method has particular potential for enabling completion of partially-excavated sections where the original support system is underdesigned.
Chapter 2 of this thesis present the general layout for the key section analyzed, introducing the problem and extensively explain the characteristic of the remedial solution proposed. Chapter 3 describes the site location and the specific soil conditions encountered in Singapore and later adopted for the analyses while Chapter 4 introduces all the main features of the key section and finite element model assumed. Chapter 5 describes a numerical study using non-linear finite element simulations, to investigate the key parameters controlling the performance of the external ground improvement system, these include: a) the vertical thickness, h, of the ground treatment zone, b) the ratio N between the undrained shear strength of the treated soil and the in situ Lower Marine Clay, c) the horizontal plan coverage, expressed as a percentage of the plan area, and d) the lateral extent of the treatment zone Δ.

The main results of the numerical study were as follow:

1. The treatment of a significant volume of soil beyond the wall (Δ>10 m, h> 16 m) significantly reduces the wall deflection and bending moment compared to the case with no treatment. However, the ground modification has much less impact on the loads carried by the strutting system except at the 7^{th} and 8^{th} strut levels.
2. The strength ratio and replacement area have much less effect on the performace of the excavation support system.

3. The proposed ground treatment cannot prevent the formation of one plastic hinge in the wall at RL 64.5 m (i.e. below the formation at a depth of 39 m). This has no impact on overall wall stability providing there is adequate capacity in the strut system.

The analyses in Chapter 5 consider a first-time excavation and do not account for the large ground movement and pre-existing wall bending history that occurred during the actual project. At the section of interest (Type K) the excavation reached a depth of 20 m with 6 levels of struts in place and wall deflections exceeding 400 mm. Chapter 6 considers the application of the same ground improvement technique as a retrofit solution to enable completion of the excavation. In this case the model includes the entire history of the excavation process, infilling after the nearby failure, installing of the grout treatment and subsequent re-excavation to final formation level.
Based on the prior parametric studies (in Chapter 5) the treatment scheme had a vertical thickness, h=20 m, a plan coverage of 50 % and an horizontal extent Δ=10 m.
This proposed remediation scheme proves to be very effective for completion of the project. The incremental wall deflections during the second excavation are up to 150 mm (at depth below 21 m) but there is no increase in the pre-existing maximum wall deflection. Apart from one deep plastic hinge, the bending moments are 35 % below the capacity of the original diaphragm wall.

7.2 Conclusions

The parametric study presented in this treatise numerically assessed the efficiency of improving soft clay mass on the external side of an existent deep excavation in Singapore with cementing agents applying specific ground improvement techniques such as jet grouting or deep mixing (see Appendix A for details on these methods). There are considerable effects in controlling the wall deflection of the wall and its bending moment; the impact on the struts and JGP axial load, are also advantageous, but are not significantly affected by the proposed ground treatment.
As a first order of estimation this solution seems to be applicable enabling to complete and control the excavation process.

The application of these methods is a real advantage for the specific case analyzed since the ground treatment can be performed in a limited working area eliminating the problem of "shut down" generally related with projects of this origin.
Real effects are obtained in controlling the behavior of the wall for a vertical thickness of the treatment higher than 16 m in the lower marine clay and a percentage of plan coverage higher than 50 %. Wall deflections are well controlled when the lateral extent of the treatment is $\Delta > 15$ m, but smaller zones ($\Delta = 10$ m) are sufficient for the current application. The choice of the final combination of the ground improvement parameters is driven by cost and time issues.
Regarding the design strength for the soil cement mix, a N ratio higher than 6 does not affect significantly the response of the structural elements of the excavation therefore in this case it is recommended to follow the practice commonly adopted in Singapore and design an improvement soil with a undrained shear strength of 300 kPa.

We are not aware of any prior application of an external ground improvement scheme to remediate deep excavations. Therefore further studies are definitely needed to evaluate risk of the proposed solution. It would be helpful to develop more comprehensive 3D models that account for the spatial arrangement of the soilcrete columns. More work is also needed to refine parameters for soilcrete. A parallel effort is also required to apply the observational method and measure closely wall movements and strut loads in the support system. In fact, in case no more detailed information is available to refine the structural model for the wall, it is nevertheless important to recommend a close monitor of the wall deflection with frequent and constant reading from inclinometers installed on the wall. From this data it is possible to make a "real-time" estimation of the bending moment acting on the wall (through curve fitting methods e.g. Ooi, Ramsey, 2003).

An efficient monitoring plan need to be assessed during the application of the treatment, avoiding therefore errors coming from lack of carefulness in the installation since the geometry is the main guide line for the solution proposed.
Significant attention needs to be put also on the monitoring of the structural elements such as walls, struts and JGP done with a series of inclinometers and strain gages installed in appropriate

locations. In case, the observational method can be applied to assure a certain amount of safety beyond the results obtained.

In general, it is computationally confirmed that the remedial solution proposed can be a good alternative to commonly used retrofit solutions but its applicability it is also limited to an existent case and can hardly represent a good alternative to traditional types of stability improvement techniques adopted for new projects for deep excavations in soft clay.

References list

Bell, B.C., and Chiew, S-P. (2006). "Nicoll Highway Collapse: Some Structural Observations: Part 2: Soil Retention System", *Proc. International Conference on Deep Excavations*, Singapore 2006, 1-15.

Burke, G.K. (2004). " Jet Grouting Systems: Advantages and Disadvantages", *Proc. of the conference Geo-Support 2004* , Orlando, Florida, 2004.

Chew, S.H., Kamruzzaman, A.H.M., and Lee, F.H. (2004). "Physicochemical and Engineering Behavior of Cement Treated Clays", ASCE *J. Geotech. Geoenviron. Eng.*, 130 (7), 696-706.

Chu, J., Bo, M.W.,Chang, M.F., and Choa, V. (2002). "Consolidation and Permeability Properties of Singapore Marine Clay", ASCE *J. Geotech. Geoenviron. Eng.*, 128 (9), 724-732.

COI (2005) "Report of the Committee of Inquiry into the incident at the MRT Circle Line worksite that led to collapse of Nicoll Highway on 20th April 2004", Ministry of Manpower, Singapore.

CDIT, Costal Development Institute of Technology, Japan (2002) " The Deep Mixing Method-Principle, Design and Construction", A.A. Balkema Publishers, Tokyo

Davies, R.V., Fok, P., Norrish, A., and Poh, S.T. (2006). " The Nicoll Highway Collapse: Field Measurements and Observations", *Proc. International Conference on Deep Excavations*, Singapore 2006, 1-15.

Essler, R, and Yoshida, H. (2004) "Jet Grouting" , Ground Improvement, 2nd Edition edited by Moseley and Kirsch, Spon Press, London and New York, 2004.

Lee, F-H., Lee, Y., Chew, S-H., and Yong, K-Y. (2005). " Strength and Modulus of Marine Clay-Cement Mixes", ASCE *J. Geotech. Geoenviron. Eng.*, 131 (2), 178-186.

Liu, J. (2003). "Compensation Grouting to Reduce Settlements of Buildings during an Adjacent Deep Excavation", *Proc. Conference Grouting 2003*, 837-844.

Liu, G.B., Ng, C.W.W., and Wang, Z.W. (2005). "Observed Performance of a Deep Multistrutted Excavation in Shanghai Soft Clays", ASCE *J. Geotech. Geoenviron. Eng.*, 131 (8), 1004-1013.

Hashash, Y.M.A. (1992). "Analysis of Deep Excavations in Clay", PhD thesis, MIT, Cambridge, Mass.

Hashash, Y.M.A., and Whittle, A.J. (2002). " Mechanics of Load Transfer and Arching for Braced Excavations in Clay", ASCE *J. Geotech. Geoenviron. Eng.*, 128 (3), 187-197.

Ho, C.E., Lim, C.H., and Tan, C.G. (2005). "Jet Grouting Applications for Large-Scale Basement Construction in Soft Clay", *Innovations in Groutig and Soil Improvement, Proc. Intern. Conference Geo-Frontier 2005*, Austin, Texas,2005.

Ho, C.E., and Tan, C.G. (2003). " Stabilization of Deep Excavations in Soft Soil by Jet Grouting", *Proc. Conference Grouting 2003*, 269-280.

Holm, G. (2000) "Deep Mixing", *Proc. Soft Ground Technology Conference*, Netherlands, 2000, 105-122.

Hsieh, H-S., Wang, C-C., and Ou, C-Y. (2003). " Use of Jet Grouting to Limit Diaphragm Wall Displacement of a Deep Excavation", ASCE *J. Geotech. Geoenviron. Eng.*, 129 (2), 146-157.

Kamon, M. (2000) "Remediation Techniques by Use of Ground Improvement", *Proc. Soft Ground Technology Conference*, Netherlands, 2000, 374-387.

Karlsrud, K., Andresen, L. (2005). "Loads on Braced Excavations in Soft Clay", *Int. Journal of Geomechanics*, 5(2), 107-113.

Long, M. (2001). " Database for Retaining Wall and Ground Movements Due to Deep Excavations", ASCE *J. Geotech. Geoenviron. Eng.*, 127 (3), 203-224.

Masuda, T. (1993). " Behaviour of Deep Excavation with Diaphragm Wall", PhD thesis, MIT, Cambridge, Mass.

Ooi, P.S.K., and Ramsey, T.L. (2003). " Curvature and Bending Moments from Inclinometer Data", *Int. Journal of Geomechanics*, 3(1), 64-74.

O'Rourke, T.D., and O'Donnell, C.J. (1997). " Deep Rotational Stability of Tieback Excavations in Clay", ASCE *J. Geotech. Geoenviron. Eng.*, 123 (6), 506-515.

Ou, C-Y., Wu, T-S., and Hsieh, H-S. (1996). " Analysis of Deep Excavation with Column Type of Ground Improvement in Soft Clay", ASCE *J. Geotech. Geoenviron. Eng.*, 122 (9), 709-716.

Page, R.J., Ong., J.C.W., Osborne, N., and Shirlaw, J.N. (2006). " Jet Grouting for Excavations in Soft Clay- Design and Construction Issues", *Proc. International Conference on Deep Excavations*, Singapore 2006, 1-18.

Peck, R.B. (1969). "Deep Excavations and Tunnelling in Soft Ground", *Proc., 7th Int. Conf. on Soil Mechanics and Foundations Engineering*, Mexico City, State of the Art Volume, 225-290.

PLAXIS (2006). *PLAXIS* version 8.2 Professional version (www. Plaxis.nl)

Raju, V.R., Schrader, D., and Minuzzo, M.(2006). " Jet Grouting in Soft Marine Clay for Deep Shaft Excavation and Tunnelling Works in Singapore", *Proc. International Conference on Deep Excavations*, Singapore 2006.

Shirlaw, J.N.(2003). " Jet Grouting Soft Clays for Tunnelling and Deep Excavations-Design and Construction Issues", *Proc. Grouting 2003*, 257-268.

Smith, I.M., and Ho, D.K. H. (1992), "Influence of Construction Technique on the Performance of a Braced Excavation in Marine Clay", *Int. J. for Numerical and Analytical Methods in Geomechanics*, 16, 845-867.

Sondermann, W., and Toth, P.S. (2000) "State of the Art of Jet Grouting Shown on Different Applications", *Proc. 4th Int. Conference on Ground Improvement Geosystems (GIGS),* Helsinki, 2000, 181-194.

Tan, T-S., Lee, F.H., Chong, P.T., and Tanaka, H. (2002). "Effect of Sampling Disturbance on Properties of Singapore Clay", ASCE *J. Geotech. Geoenviron. Eng.*, 128 (11), 898-906.

Ukritchon, B., Whittle, A.J., and Sloan, S.W. (2003). "Undrained Stability of Braced Excavations in Clay", ASCE *J. Geotech. Geoenviron. Eng.*, 129 (8), 738-754.

Wen, D., Song, S.K., Goh, K.H., and Lin, K.Q. (2006). "Design Approaches to Temporary Retaining Walls for Stability", *Proc. International Conference on Deep Excavations*, Singapore 2006, 1-8.

Whittle, A.J., and Davies, R.V. (2006). "Nicoll Highway Collapse:Evaluation of Geotechnical Factors Affecting Design of Excavation Support System", *Proc. International Conference on Deep Excavations*, Singapore 2006, 1-16.

Wong, K.S., and Poh, T.Y. (2000). " Effects of Jet Grouting on Adjacent Ground and Structures", ASCE *J. Geotech. Geoenviron. Eng.*, 126 (3), 247-256.

Wong, K.S., and Goh, A.T.C. (2006). "Modelling JGP Slab in Deep Excavation Analysis", *Proc. International Conference on Deep Excavations*, Singapore 2006.

Yong, K.Y., Teh, H.S., and Wong, K.S. (2006). "System Failure of Temporary Earth Retaining Structure Leading to Collapse of Nicoll Highway", *Proc. International Conference on Deep Excavations*, Singapore 2006, 1-16.

Appendix A

GROUND IMPROVEMENT TECHNIQUES

It is widely known in the engineering world that structures need to be built in locations presenting good ground conditions. However, occasionally it is not possible to bypass the problem by changing the project's location or by the use of deep foundations. As a consequence, ground improvement techniques applied in the geotechnical engineering practice, are useful tools to solve problems of poor ground conditions.

Over the years a lot of new methods have been develop to face different types of practical problems needed soil improvement. In particular, ground improvement in soil has been used to achieve to five major functions (Munfakh, and Wyllie, 2004):

- to increase the bearing capacity
- to control deformations and accelerate consolidation
- to provide lateral stability
- to form seepage cut-off and environmental control
- to increase resistance to liquefaction

In order to accomplish these functions, as said, a wide range of soil improvement methods exist and they may be divided in different categories:

- Densification
- Consolidation
- Weight reduction
- Reinforcement
- Chemical treatment
- Thermal stabilization
- Electrotreatment
- Biotechnical stabilization

Each of these methods applied to specific types of soil and functions. Table A.1 relates the different techniques cited to the soil conditions and purposes they are applied for.

Table A.1- Ground Improvement methods and their main objectives *(Munfakh, and Wyllie, 2004)*

Ground Improvement Method	Type of Soil		Ground Improvement Objectives				
	Granular	Cohesive	Bearing Capacity	Settlement Control	Lateral Stability	Environmental Control	Liquefaction Resistance
Vibrocompaction	•		•	•			•
Dynamic Compaction	•		•	•		•	•
Blasting	•		•	•			•
Compaction Grouting	•			•			
Preloading/ Drains		•	•	•			•
Electro-osmosis		•	•	•			
Vacuum Consolidation		•	•	•			
Lightweight Fill	•	•		•			
Mechanical Stabilization	•		•	•	•		
Soil Nailing	•				•		
Soil Anchoring	•				•		
Micropiles	•		•	•	•		
Stone Columns		•	•	•	•		•
Fiber Reinforcement	•		•	•	•		
Permeation Grouting	•		•	•		•	
Jet Grouting	•	•	•	•	•	•	•
Deep Soil Mixing	•		•	•	•	•	•
Lime Columns		•	•	•	•	•	•
Fracture Grouting		•	•	•		•	
Ground Freezing	•	•			•	•	
Vitrification	•	•				•	
Electrokinetic Treatment		•		•		•	
Electroheating		•		•		•	
Biotechnical Stabilization	•				•	•	

Following, a brief description of the methods previously categorized is given with a more detailed explanation on the jet grouting and deep soil mixing methods.

- Ground improvement by *Densification*

For loose granular soils, densified in order to increase the bearing capacity (foundations problems), reduce settlements and increase resistance to liquefaction. When applied at the surface conventional rollers are used while, if the improvement is necessary at depth densification is obtained using vibrocompaction, dynamic compaction, blasting or compaction grouting.

- Ground improvement by *Consolidation*

Consolidation of soft cohesive soil improved the engineering properties of the soil itself. Through the consolidation process both the strength and unit weight of soil are increased while the hydraulic conductivity is reduced. Problems that may arise are the decrease in volume after consolidation causing potential risk for ground deformations. Methods of consolidation improvement are preloading with or without vertical drains, electro-osmosis and vacuum consolidation.

- Ground improvement by *Weight Reduction*

This method simply consists in the reduction of the weight applied to an underlain soil by the use of lightweight fill material. This method permits to reduce settlements, increase slope stability and reduce lateral earth pressure on retaining structures.

- Ground improvement by *Reinforcement*

The soil is reinforced, mainly with mechanical techniques, by inclusion of reinforcing elements in the soil. These methods applied for settlement control problems, to improve resistance to liquefaction or to strengthen the soil in general. The reinforcement is accomplished with mechanical stabilization, soil nailing, soil anchoring, micropiles, stone columns and fiber reinforcement.

- Ground improvement by *Chemical Treatment*

Different cementing agents are used to stabilize weak soils such as cement or lime; these agents bind the soil particles creating a new mix, generally called soilcrete, with higher strength values and lower compressibility. In surface stabilization, the chemicals are mixed with the soil and a certain amount of water and then compacted with the traditional techniques; when at depth, the treatment is applied by injection or by deep mixing methods. The typical techniques for chemical treatment are permeation grouting, jet grouting, deep soil mixing, lime columns and fracture grouting.

➢ Ground improvement by *Thermal Stabilization*

Both heating and freezing can be used to stabilized soil even if heating techniques are still in an experimental phase. Ground freezing is the most widely used method of thermal stabilization especially in application in urban areas.

➢ Ground improvement by *Electrotreatment* and *Biotechnical Stabilization*

These two types of ground improvement are mainly used for environmentally sensitive area for purposes such as remediation of contaminated sites or stabilization of slopes when the attention to the environment is one of the main concern in the project.

A.1 Jet Grouting

A.1.1 Introduction

Among all the different methods of ground improvement nowadays existent in the market, jet grouting might be considered one of the most versatile. At the same time it is also one of the most technically demanding requiring considerable care both in the design and construction phases.

Jet grouting has a long history of development from the first time it has been since until now. The most notable progress has taken place in Japan. This technology was initially adopted to improve the effectiveness of water tightness in chemical grouting and subsequently it has been applied to create cut-off walls and prevent water ingress. At this stage, jet grouting was mainly applied in form of panels; it is only in the 1970's that in Japan a more versatile form of jet grouting started to develop: rotating jet grouting (Essler et al., 2004).

At the present time the jet grouting technique is used in Europe for more than 20 years, initially in a sporadic way but recently the technique is commonly applied to solve different kinds of problems, such as:

- deeping of existing foundations
- retaining wall of large excavations

- installation of sealing screens or blocks, especially for tunneling projects

A.1.2 Application and Construction Issues

There are three traditional jet grouting systems as illustrated in figure A.1.Consideration on the function that the improvement needs to achieve, on the properties of the in situ soil determine the selection of one of the systems proposed.

–Single Fluid System: the disaggregation and cementation of soil is obtained by the injection at high energy of a cementitious grout slurry. This energy causes the erosion of the ground and the placement and mixing of grout in the soil.

–Double Fluid System: a two-phase internal rod system is employed for the separate supply of grout and air (sometimes water) to cement the soil and the grouted slurry. The main purpose of the air is to increases erosion efficiency. The double rod system is more effective in cohesive soils than the single rod system.

–Triple Fluid System: the erosion and disaggregation of the soil is obtained by an high energy water jet assisted by an air jet shroud while simultaneously grout slurry is injected from beneath the erosion sets. Triple-rod jet grouting is the most effective system for cohesive soils.

The process of jet grouting is in most cases "bottom-up" meaning the use of hydraulic rotary drilling to reach the design depth, then water or a cement agent is pumped through one or more nozzles at high pressure, generally 300 to 600 bar (figure A.2). The spoil return normally flows to the ground surface via the annulus of the jetting hole. Any obstruction to the free flowage of the spoil may determine an over-pressure on the ground and potential ground heave.

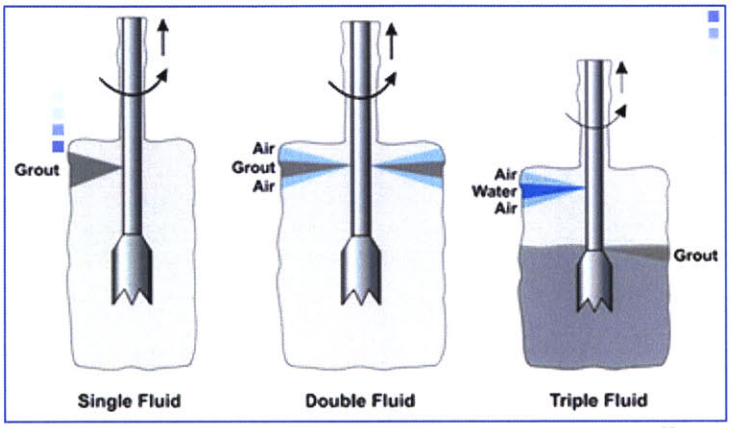

Figure A.1-The three most common jet grouting systems

(Hayward Baker (A Keller Company), 1/4/2007)

Although jet grouting may works in most types of soils (figure A.3), because the initial structure of the soil is almost completely broken by the erosion process, it s success is significantly influenced by the ground characteristics and conditions. Therefore soil erodibility plays a major role in predicting geometry and quality of the system. Cohesionless soils are most easily eroded and as plasticity and stiffness increase, erodibility decreases to a point where jet grouting will not be effective in most stiff clays.

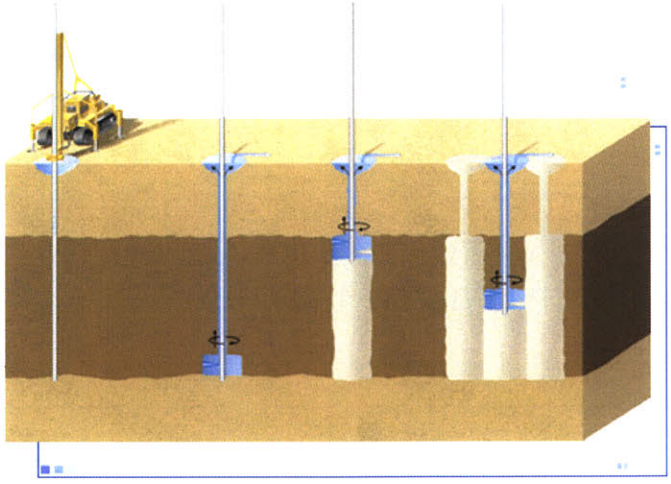

Figure A.2-The jet grouting process

(Hayward Baker (A Keller Company), 1/4/2007)

In particular, gravels and boulders, even if they are considered cohesionless materials, they can be very difficult to erode and might block the jet stream.

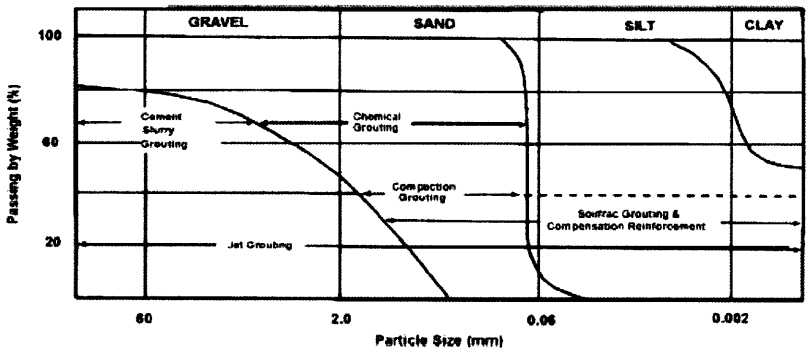

Figure A.3-Range of groutable soils

(Munfakh et al, 2004)

The main parameters controlling the use of jet grout in a special project and in particular the cross sectional dimensions and the strength of the grouted elements are:

-pressure of the fluids

- flow rate of the fluids

-mass of the flids

-rotation and lift speed of the jet grouting string

-viscosity of the fluid

-velocity of the fluid.

-position of the drilling starting point

These parameters are often controlled by the equipment, from preparation of the fluid to the pumping pressures and volumes. A good quality control is highly recommended to achieve the best correspondence between the design values used and the in situ obtained engineering properties.

Jet Grouting can be installed at any depth and can be pinpointed in specific strata. The width or diameter of each panel or column and size of soilcrete mass that needs to be created is

determined during the design stage. Example of soilcrete plan geometry are presented in figure A.4.

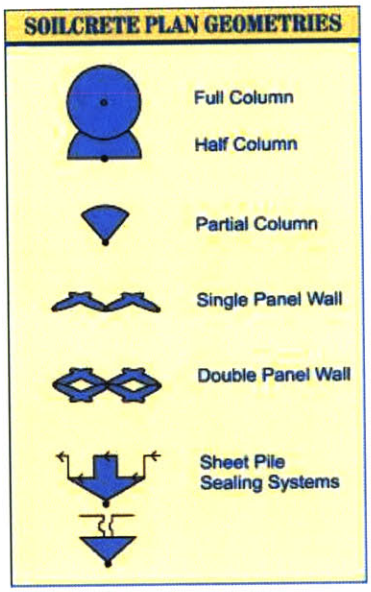

Figure A.4-Soilcrete plan geometries

(Hayward Baker (A Keller Company), 1/4/2007)

In order to successfully design a jet grout project, a series of issues both in the design and construction phase need to be assessed.

First of all it is important to determined the strength of treated ground and this usually is done referring to results from unconfined compressive strength tests on samples obtained by coring. A series of useful charts have been adopted by the Japan Jet Grouting Association in order to give recommendations on the unconfined compressive strength to be taken, for different types of soils, in design (Essler, et al.,2004).

Moreover, even drilling tolerances are important, especially when the design requires overlapping of columns. In fact, inadequate interlocking due to drilling deviation, not only increases the offset from neighboring columns but it might also cause the penetration of the new column into a column already in place.

These problems can easily be addressed with good drilling and hole survey techniques.

In order to well manage the entire process of grouting, it is also equally important to carry out quality control testing on the grouts used such as specific gravity, viscosity and strength of the cube after 28 days. Knowing these parameters it is fundamental if improvement measures need to be taken to assure a certain amount of safety to the project in case a column has been either misplaced or incorrectly installed.

A.2 Deep Mixing Method

A.2.1 Introduction

The deep mixing technology using dry or wet binder materials goes back more than 30 years. Research and practical development on this field started in the mid 1960's in Sweden at the Swedish Geotechnical Institute and in Japan at the Port Harbor Research Institute (Holm, 2000). This type of mechanical mixing has been developed for mixing stabilizers under deep ground conditions without excavation, shoring, or dewatering; thus, having relatively low cost and allowing less exposure of waste. This method is commonly abbreviated as DMM. Initially quicklime was used as stabilizing agent while in modern times Portland cement is more adopted both in slurry and dry state.[1]

The Deep Mixing Methods, as other ground improvement method, have been employed for different purposes such as (Holm, 2000):
-reduction of settlements
-increase of stability
-prevention of sliding failure
-protection of structures close to excavation sites
-reduction of vibration
-liquefaction mitigation
-remediation of contaminated ground

[1] Portland cement is more compatible with Japanese clay soils and Japan widely uses this method of improvement (Kamon, 2000)

A.2.2 Application and Construction Issues

Deep mixing can act as a bearing element or as soil improvement interacting with the unstabilized soil. Columns of different diameters and strength, walls, grids or blocks can be obtained through the process. In particular the columns can be designed with very high strength and in that case they perform the function of bearing element demonstrating brittle behavior and very low strain at failure; in some other cases they can have an appropriate strength level and interact with the unstabilized soil between them (semi-hard column).

By mixing the binder agent with the soft soil, it is possible to improve different engineering properties. This change is related to various factors and in particular it depends on the characteristics of the soil layers, of the binders, on the mixing conditions and procedure and finally on the curing conditions (temperature, humidity, curing time).

In fact, an important characteristic of stabilized soil is the long-term increase in strength, mainly depending on the type of binder used; in particular, in some areas like in Sweden for example, to avoid problems of long-term creep settlements a preloading procedure is used consisting in the application of a temporary surcharge to allowed settlements during the construction phase (Holm, 2000).

In situ DMM techniques are applicable to a various range of soft alluvial and marine soils, organic soils and for reclamation fill. In particular, almost every type of shape con be obtained through different combinations and overlapping of the columns (figure A.5) as a function of the purpose of the intervention.

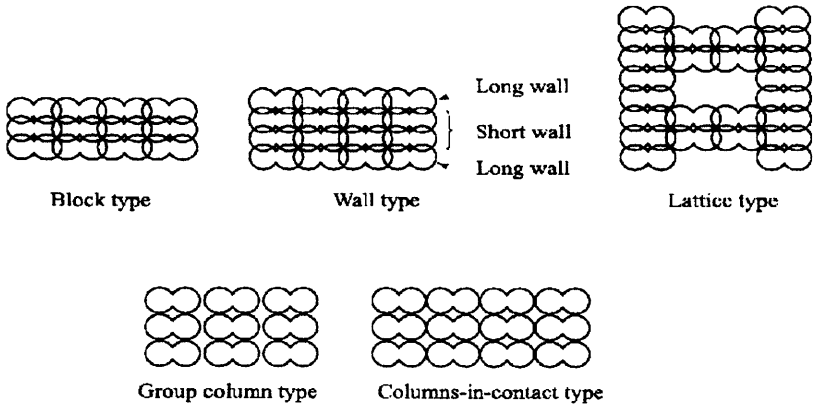

Figure A.5- Characteristics of improved types and typical arrangement patterns

(CDIT, 2002)

Referring to the application process, the first step to be done before starting with the design is to assess the properties of the unstabilized soil by field and laboratory tests in order to make the best choice of the binder and its combination with the in situ soil. Figure A.6 clearly evidences the complete procedure adopted to obtain the best results in the application of this technique.

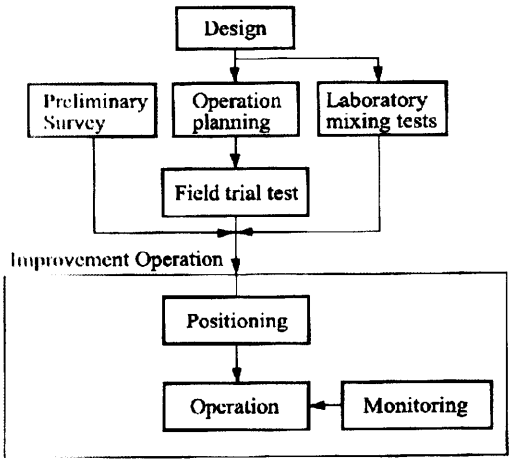

Figure A.6- Typical DM method construction

(CDIT, 2002)

The DMM method, as said before, can be applied both for marine and on land works; construction procedure for the marine and on land works respectively is represented in figure A.7.

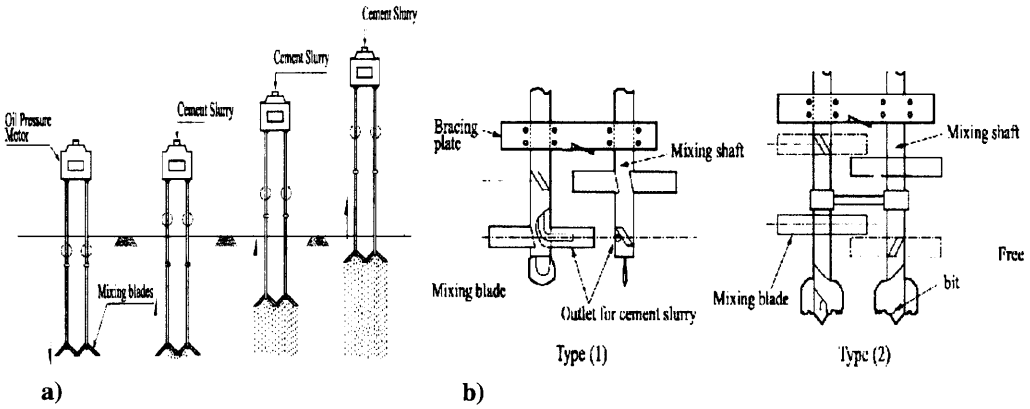

Figure A.7- Construction procedure for marine works (a) and on land works (b)

(CDIT, 2002)

For both cases, the improvement operation comprises of sinking the machine into the soft ground under its self weight. In the withdrawal stage of the machine, the stabilizing agent in the slurry form is injected into the soil and the mixing blades mix the soft soil and the stabilizing agent to form a uniform mixture.

Quality control for DMM is important not only in the initially phase but should performed during the entire construction process to verifying the behavior of the whole soil improvement. Normally the measures include settlements, pore pressures and sometimes also horizontal movements. As explained from figure A.6, the design should often include planned actions to take depending on the measurements results (observational method).

Appendix B

GEOMETRY OF THE FINITE ELEMENT MODEL, DETAILS

It this appendix details on the geometry and characteristics of the finite element model, for the entire process of excavation, adopted to compute the efficiency of the solution proposed.

B.1 General Settings

General

Plane-Strain
15- Nodes

Mesh[1]

Number of Elements: 458
Number of Nodes: 3908
Number of Stress Points: 5496
Average element size: 4.74 m

B.2 Input

Geometry Model

The problem can be modeled with a geometry model of 100 m width and 102.9 m height.
The steel struts are modeled as *fixed-end anchors.*
The diaphragm wall is modeled as *plate*. The *interfaces* around the plates are used to model soil-structure interaction effects.
The excavation is constructed in ten excavation stages. The separation between the stages is modeled by geometry lines.

[1] Mesh automatically generated

The *standard fixities* are used to generate the proper boundary conditions.

The proposed geometry model is given in figure B.1.

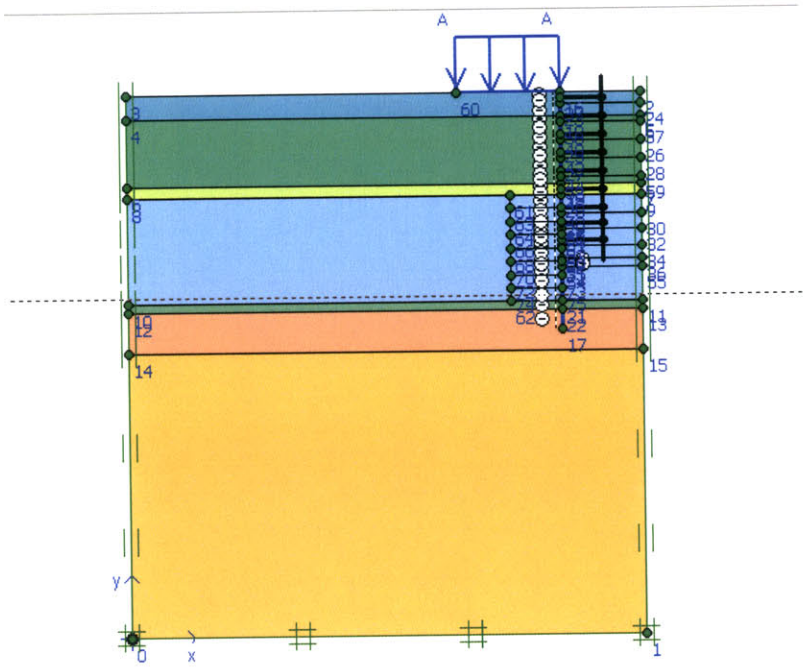

Figure B.1-Geometry model of excavation

PLAXIS

Material Properties

Table B.1 to B.3 list the properties of the materials adopted for the model. In particular, table B.1 refers to soil properties, table B.2 to properties of the diaphragm wall, and table B.3 to properties of the anchors.

For all the different type of soil in the model a Mohr-Coulomb linear elastic perfectly plastic behavior is assumed.

Other assumptions made are:

-the type of material behavior is assumed to be always undrained with no friction except for the fill, assumed drained with effective friction angle;

- the soil unit weight above phreatic level γ_{unsat} and below phreatic level γ_{sat} are considered equal (the soil in fact is always in a saturated condition along the various stages of excavation);
- every layer is considered isotropically permeable therefore horizontal and vertical permeability (hydraulic conductivity) have equal value.

Table B.1- Soil Profile

Soil Layer	RL (m)	γ (kN/m^3)	s_u (kPa)	ϕ'	G (Mpa)	ν'	k (m/day)	k_0	H (m)
Fill	102.9	19	0	30	4	0.25	0.086	0.5	100.5
Upper MC	98.2	16	20 25	0	3	0.25	8.6*10-5	0.7	100.5
F2 Clay	85.6	19	88	0	11.7	0.25	8.6*10-5	0.7	103
Lower MC	83.4	16.8	31 47	0	5.2	0.25	8.6*10-5	0.7	103
F2 Clay	63.2	20	88	0	11.7	0.25	8.6*10-5	0.7	103
OA weathered	61.6	20	100 500	0	40	0.25	8.6*10-4	1	103
OA competent	53.9		500	0	67	0.25	8.6*10-5	1	103
JGP		16	300	0	108	0.15	8.6*10-5		

Chapter 7 comments on the results obtain for the case of a ground treatment consisting in columns 20.2 m high, covering the entire layer of LMC and with a coverage in plan of 50 %. An equivalent strength resistance has been used as input value with the hypothesis that the properties of the cement-soil mix are the same as the one originally used to build the JGP slab. In particular, since the undrained shear strength of the soil is 300 kPa, for a coverage of 50 %, an equivalent layer having half the resistance (150 kPa) and 100 % plan coverage is input. Other elasticity properties do not change.

Table B.2- Properties of Diaphragm wall

Diahragm Wall	
Type of Behavior	Elastic
Normal Stiffness EA	$2.24*10^{+7}$ kN/m
Flexural Rigidity EI	$8.36*10^{+5}$ kNm^2/m
Weight w	6.4 kN/m/m
Poisson's Ratio	0
Maximum Yielding Moment Mp	2300 kNm/m
Thickness d	0.8 m

The wall extent from ground level RL 102.9 to RL 57.9 m for a total length of 45 m, embedded in the lower 8 meters of lower marine clay and with the toe located in the Old Alluvium. The

distance between the walls in plan view is of 31 m but in the model, due to the symmetry of the problem, only half excavation has been considered.

Table B.3a and B.3b plot the properties of the struts for the initial excavation process, with no improvement (Table B.3a) and for the new excavation process after the treatment has been installed. In the sequence of the stages the new struts substitute the old ones, still in place. It is evident to notice that the preload apply to the new struts is much lower than the ones for the initial excavation while the maximum compressive capacity is also increased. For the purpose of the exercise, conventional steel HE beams are used.

Table B.3a- Properties of the struts, initial excavation

Strut Level	Dimensions (mm)	EA (kN/m)*10^6	Installation Depth (m)	Preload (kN/m)	F_{max} (kN)
1	H344	0.9	RL-1.1	150	825
2	H400	1.15	RL-4.6	200	975
3	H414	1.55	RL-8.1	450	1200
4	H414	1.55	RL-11.6	600	1200
5	H414	1.55	RL-15.1	600	1200
6	H414	1.55	RL-18.6	600	1200
7	2H414	3.1	RL-21.9	750	2400
8	2HR400	2.1	RL-24.9	600	1950
9	H414	1.55	RL-28.1	400	1200

Table B.3b- Properties of struts, after treatment

Strut Level	Dimensions (mm)	EA (kN/m)*10^6	Installation Depth (m)	Preload (kN/m)	F_{max} (kN)
1	H344	0.9	RL-1.1	200	825
2	H400	1.15	RL-4.6	200	975
3	HEA260	1.788	RL-8.1	600	1800
4	HEA260	1.788	RL-11.6	600	1800
5	HEA280	2	RL-15.1	600	2140
6	HEA280	2	RL-18.6	600	2140
7	2HEA260	3.576	RL-21.9	600	3600
8	2HEA260	3.576	RL-24.9	600	3600
9	HEA260	1.788	RL-28.1	400	1800

Also a vertical distributed load of 20 kN/m^2 extending for 20 m behind the diaphragm wall is considered to take into account the load due to working equipment.

The water table is at ground level (RL 102.9 m) and the excavation takes places in dry condition. Dynamic effects due to groundwater flow are not taken into account due to the very low permeability of the soil layers.

B.3 Calculations

Excavation processes are modeled with PLAXIS with the special option *Staged Construction* which enable the activation or deactivation of different components in the model.
The analysis is done in 40 calculated phases, which are listed below; after each excavation stage there is the application of an horizontal point loads at the strut ends, which represent the pre-stress force on the strut itself. As soon as the initial excavation process reaches the 6^{th} level (RL 83.3 m), a backfilling process starts, divided in 5 phases. Once the entire trench has been backfilled the ground treatment is installed externally to the excavation and the process starts again until the bottom of the excavation is reached.
Before the actual excavation takes place, in the first stages there is the installation of the diaphragm wall and the activation of the vertical load.
Table B.4 summarize the entire process.

Table B.4- Construction phases

Stage	Construction Activities	Stage	Construction Activities
1	Diaphragm wall installation	21	Ground improvement treatment installation
2	Distributed load activation	22	Excavate to RL-2.1m
3	JGP slab installation	23	Install and preload 1st level of strut
4	Excavate to RL-2.1m	24	Excavate to RL-5.6m
5	Install and preload 1st level of strut	25	Install and preload 2nd level of strut
6	Excavate to RL-5.6m	26	Excavate to RL-9.1m
7	Install and preload 2nd level of strut	27	Install and preload 3rd level of strut
8	Excavate to RL-9.1m	28	Excavate to RL-12.6m
9	Install and preload 3rd level of strut	29	Install and preload 4th level of strut
10	Excavate to RL-12.6m	30	Excavate to RL-16.1m
11	Install and preload 4th level of strut	31	Install and preload 5th level of strut
12	Excavate to RL-16.1m	32	Excavate to RL-19.6m
13	Install and preload 5th level of strut	33	Install and preload 6th level of strut
14	Excavate to RL-19.6m	34	Excavate to RL-22.9m
15	Backfill to RL-16.1 m	35	Install and preload 7th level of strut
16	Backfill to RL-12.6 m	36	Excavate to RL-25.9m
17	Backfill to RL-9.1 m	37	Install and preload 8th level of strut
18	Backfill to RL-5.6 m	38	Excavate to RL-29.1m
19	Backfill to RL-2.1 m	39	Install and preload 9th level of strut
20	Backfill to ground level	40	Excavate to RL-31.6m

It is important to evidence few notes on specific phases:

- Phase 1: a specific option is selected to ignore undrained behavior of the soil during the installation of the wall;
- Phase 4: All the displacement from the previous three stages are reset to zero in order not to take into account the impact of the construction of the wall in the computed results;
- Phase 14: the staged construction procedure is controlled by a total multiplier ($\Sigma Mstage$); this multiplier generally starts at zero and is expected to reach the ultimate level of 1.0 at the end of the calculation phase. In some special situations, however, it might be necessary to split the staged construction process into more than one calculation phase and to specify an intermediate value of $\Sigma Mstage$ (*PLAXIS* Reference Manual, page 4-20). In this case, the goal was to model the wall reaching a maximum wall deflection of 400 mm at the end of this phase, since this is the value recorded by the inclinometers adjacent to the wall. A $\Sigma Mstage$ value of 0.62 has been input.

In general, after every excavation the water table was lowered to the new level of excavation and hydrostatic condition of flow were always considered.